

Targeted BACE-1 inhibition in microglia enhances amyloid clearance and improved cognitive performance

Neeraj Singh, Brati Das, John Zhou, Xiangyou Hu, Riqiang Yan*

Abnormal accumulation of β -amyloid ($A\beta$) peptides is a culprit in Alzheimer's disease (AD); blocking $A\beta$ generation is therefore being explored as a logical approach for AD treatment. Here, we demonstrate that targeted inhibition of β -site amyloid precursor protein (APP) cleaving enzyme-1 (BACE-1) in microglia has unique advantages. When *Bace-1* was deleted in Alzheimer's 5xFAD microglia, fewer amyloid plaques developed, and this reduction was not due to changes in APP processing but rather to enhanced $A\beta$ clearance, in line with the increase in a microglial gene signature favoring phagocytosis. Moreover, deletion of *Bace-1* in microglia enhances functions of autophagolysosomes and $A\beta$ -induced metabolic reprogramming necessary for $A\beta$ degradation by favoring phosphorylation of mammalian target of rapamycin complex (mTOR) at Ser²⁴⁴⁸ and modulating the PI3K-mTOR-HIF-1 α signaling pathways. Mice with deletion of *Bace-1* in microglia showed no reduction in long-term potentiation, unlike global deletion of *Bace-1*. Our results suggest that targeted inhibition of BACE-1 in microglia is a superior strategy for AD treatment.

Copyright © 2022
The Authors, some
rights reserved;
exclusive licensee
American Association
for the Advancement
of Science. No claim to
original U.S. Government
Works. Distributed
under a Creative
Commons Attribution
NonCommercial
License 4.0 (CC BY-NC).

INTRODUCTION

It has been long established that BACE-1 [β -site amyloid precursor protein (APP) cleaving enzyme-1] functions as the Alzheimer's β -secretase, and elevated neuronal BACE-1 activity is recognized to facilitate β -amyloid ($A\beta$) generation and formation of amyloid plaques in the brains of patients suffering from Alzheimer's disease (AD). Inhibition of BACE-1 is therefore being pursued to reduce amyloid deposition and accumulated amyloid plaques, which are viewed as an early pathological event in AD (1). Brain-penetrable BACE-1 inhibitors have been developed, and clinical trials of five different BACE-1 inhibitors have shown to decrease $A\beta$ production in humans (2–4). However, despite an appreciable reduction in $A\beta$ load, patients with AD taking these drugs failed to show cognitive benefits (5), and rapid loss of hippocampal volume was also noted (6). The inability of BACE-1 inhibitors to improve cognitive functions is consistent with prior studies in *Bace-1*-null mice or conditional deletion mouse models, which established the important role of *Bace-1* in synaptic functions and proper hippocampal axonal organization (7–12). Considering this setback, alternative approaches for targeted BACE-1 inhibition have been explored.

In our previous study using *Bace-1* conditional knockout mice that have deleted *Bace-1* in the adult Alzheimer's 5xFAD mouse model under the control of ubiquitin promoter, we noted that preexisting amyloid plaques could be removed (8). This observation prompted us to ask whether *Bace-1* in microglia has a role in removing amyloid plaques. To answer this question, we bred *Bace-1* flox mice (*Bace-1*^{f/f}) with mice engineered to express *Cre* recombinase under the control of Cx3Cr1 promoter via the tamoxifen-inducible (13) system to delete *Bace-1* in 5xFAD mouse microglia. The compound offspring were examined for the impact of *Bace-1* deletion on amyloid deposition and/or cognitive functions.

We demonstrated herein that conditional deletion of *Bace-1* in adult 5xFAD mouse microglia reduced amyloid plaque load, not only through enhanced $A\beta$ uptake but also via more effective clearance of engulfed $A\beta$ through effective autophagolysosomal degradation machinery. We found that targeted deletion of *Bace-1* in microglia improved synaptic strength and memory behaviors. Deletion of *Bace-1* in wild-type (WT) mouse microglia did not disrupt long-term potentiation, a synaptic phenotype seen in mice with global *Bace-1* deficiency or inhibition. Together, our study demonstrates that the specifically targeted inhibition of BACE-1 in microglia will likely offer a superior therapeutic alternative for improving AD outcomes, circumventing the safety concerns associated with neuronal deletion or global inhibition of BACE-1.

RESULTS

Aggregated $A\beta$ induces *Bace-1* expression in activated microglia

It was previously reported that BACE-1 expression is elevated in AD brains (14) and surrounding amyloid plaques (15). We found that activated microglia from 3-month-old 5xFAD mouse brains showed strong colocalization of BACE-1 with ionized calcium-binding adapter molecule 1 (IBA-1), while BACE-1 expression in microglia was barely detectable in brain sections prepared from WT mouse brains (Fig. 1A). Taking the advantage of generated results from single-cell RNA sequencing (RNA-seq) on CD11b⁺ immune cells using 2-month-old 5xFAD mice (16), we compared *Bace-1* expression in different brain cells to those of WT littermates. We showed that *Bace-1* expression was visibly higher in *Siglech*⁺ microglia (Fig. 1B), and this was confirmed by quantification (roughly by 50%; fig. S1A). It was also evident that *Bace-1* was up-regulated in stage 1 disease-associated microglia (DAM-1) microglia at the mRNA level (fig. S1B).

To determine whether oligomerized or aggregated $A\beta$ during the growth of amyloid plaques induces *Bace-1* expression in microglia, we treated purified primary microglial cells with oligomeric $A\beta_{1-42}$ for various time points. A time-dependent up-regulation of *Bace-1* mRNA was detectable in primary microglial cultures as early as 4 hours

Department of Neuroscience, UConn Health, 263 Farmington Avenue, Farmington, CT 06030-3401, USA.

*Corresponding author. Email: riyan@uchc.edu

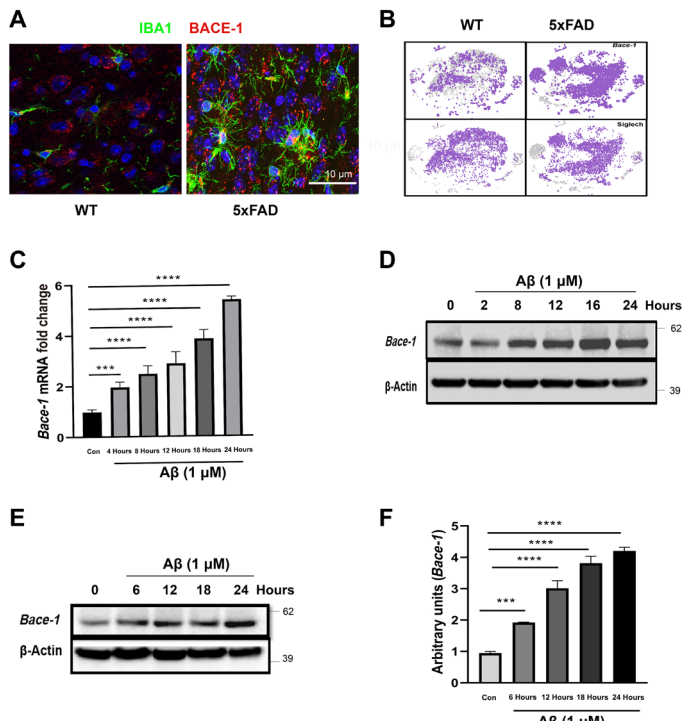


Fig. 1. Increased BACE-1 expression in Aβ-activated microglia. (A) Fluorescent immunolabeling revealed colocalization between BACE-1 (red) and the microglial marker IBA1 (26) in the frontal cortex of 3-month-old 5xFAD mouse brains. Scale bar, 10 μm. (B) Bace-1 expression in Siglech-positive microglia, derived from the brains of 2-month-old WT and 5xFAD mice via single-cell RNA-seq and expressed as median-normalized average. $N = 3$, ~5000 cells per genotype. (C and D) Primary microglial cultures were treated with A β_{1-42} (1 μM) for the indicated time periods. Reverse transcription polymerase chain reaction (RT-PCR) analysis and Western blotting were performed to compare Bace-1 mRNA (C) and protein levels (D). The normalized fold increase in Bace-1 gene expression compared to the control group was calculated by the $\Delta\Delta Ct$ method. (E) Immortalized BV-2 microglial cells were similarly treated with A β_{1-42} (1 μM) and protein lysates were used to measure BACE-1 protein levels. Bar graph shows densitometric analysis of BACE-1 normalized to β-actin (E). Data are presented as means ± SEM for each group (**P < 0.001 and *P < 0.05, Student's t test) (F).

of treatment (*P < 0.05 and ***P < 0.001; Fig. 1C). Western blot analysis showed significant increases in BACE-1 protein levels starting at 8 hours in primary microglial cultures (Fig. 1D). We also confirmed this up-regulation using a BV-2 microglial cell line (Fig. 1, E and F). Hence, BACE-1 is elevated in AD microglia cells, and this elevation likely impairs phagocytic functions of microglia as discussed in our recently published article (16).

Targeted deletion of Bace-1 in microglia reduces amyloid plaques in 5xFAD mice

With the knowledge that microglial BACE-1 is up-regulated in 5xFAD microglia, potentially by oligomerized Aβ, we asked whether specific deletion of Bace-1 in microglia would affect Aβ clearance. We bred 5xFAD;Bace-1^{f/f} mice with Cx3cr1^{CreER} mice to generate 5xFAD;Bace-1^{f/f};Cx3cr1^{CreER} mice. Amyloid plaques first developed at around 2 months of age in 5xFAD mice (17), and 5xFAD;Bace-1^{f/f};Cx3cr1^{CreER} mice were therefore treated with Tamoxifen (TAM) or left untreated for 5 days beginning at this age to delete Bace-1 in

microglia right after plaque development. TAM treatment of Bace-1^{f/f};Cx3cr1^{CreER} mice for 5 days selectively deleted Bace-1 in microglia (as shown in fig. S2, A to E). After growing for one or three additional months, mice were then euthanized at the age of 3 or 5 months for measuring amyloid plaque loads in forebrains and levels of APP processing products, including Aβ.

As shown in Fig. 2A, deletion of Bace-1 in microglia resulted in significantly fewer amyloid plaques in TAM-treated 5xFAD;Bace-1^{f/f};Cx3cr1^{CreER} mouse brains at both 3 and 5 months compared to vehicle-treated controls. We further confirmed these histochemical results by quantifying thioflavin S-positive amyloid plaques, counted manually in both cortex and hippocampus, at 3 and 5 months. At 3 months, Bace-1 deletion in microglia reduced the number of amyloid plaques by ~40% (210 ± 23 versus 131 ± 15) in the cortex and ~45% (54 ± 8 versus 29 ± 3) in the hippocampus, respectively (Fig. 2B). When quantifying by measuring the plaque density, the reduction was by ~34% (0.83 ± 0.03 versus 0.56 ± 0.04 of defined area) in 3-month-old mouse brains ($N = 6$ pairs of animals, ***P < 0.001; Fig. 2C).

While most comparative studies have been performed using female mice, we assessed potential gender effects on plaque loads in the 5-month-old mouse group. Despite of lower plaque loads in male than female 5xFAD mice, plaque numbers in cortex and hippocampus of TAM-treated 5xFAD;Bace-1^{f/f};Cx3cr1^{CreER} mouse brains were consistent: reduced by ~24% in females (820 ± 31 versus 663 ± 25) and ~32% in males (404 ± 8 versus 277 ± 34) compared to their non-treated littermates (Fig. 2D). This indicates no major effects of gender on plaque reduction. TAM-treated 5xFAD;Bace-1^{f/f};Cx3cr1^{CreER} mice similarly exhibited reduced area occupied by plaques by ~21% in females (2.45 ± 0.13 versus 1.94 ± 0.14 ; Fig. 2E) and ~48% in males (1.19 ± 0.14 versus 0.62 ± 0.09 ; Fig. 2F), respectively. Noticeably, the overall plaque loads were higher in 5-month-old mice compared to 3-month-old 5xFAD;Bace-1^{f/f};Cx3cr1^{CreER} mice, and this was likely because neuronal BACE-1 continued to produce Aβ in an age-dependent manner.

Targeted deletion of Bace-1 in 5xFAD mouse microglia enhances Aβ removal

Because Bace-1 is largely expressed by neurons and is less expressed by glial cells, specific deletion of Bace-1 in microglia did not visibly result in changes in BACE-1 protein levels in 3-month-old female TAM-treated 5xFAD;Bace-1^{f/f};Cx3cr1^{CreER} brains compared to controls (Fig. 3A). Consistently, TAM-treated 5xFAD;Bace-1^{f/f};Cx3cr1^{CreER} mice had similar levels of full-length APP and APP-C99, a 99-amino acid-long membrane-bound C-terminal fragment of APP cleaved by BACE-1, to those of corn oil-treated 5xFAD;Bace-1^{f/f};Cx3cr1^{CreER} mice (Fig. 3A). Similar results were seen in 3-month-old male mice (fig. S3, A and B). We also examined brain lysates from 5-month-old female mice, and no changes in APP processing to C99 by BACE-1 were noticeably detected (Fig. 3, C and D). However, we noted a reduction in astrogliosis, as reflected by measuring glial fibrillary acidic protein levels with SMI22, which is in line with reduced amyloid plaques in TAM-treated 5xFAD;Bace-1^{f/f};Cx3cr1^{CreER} mice. These immunoblot results confirm that APP processing by BACE-1 was not noticeably altered when Bace-1 was deleted only in microglia.

When Aβ levels were examined via Western blot, we found that Aβ migrating near 5 kDa were reduced in Bace-1-deleted 5xFAD;Bace-1^{f/f};Cx3cr1^{CreER} mice (Fig. 3, A and B). Both soluble and insoluble

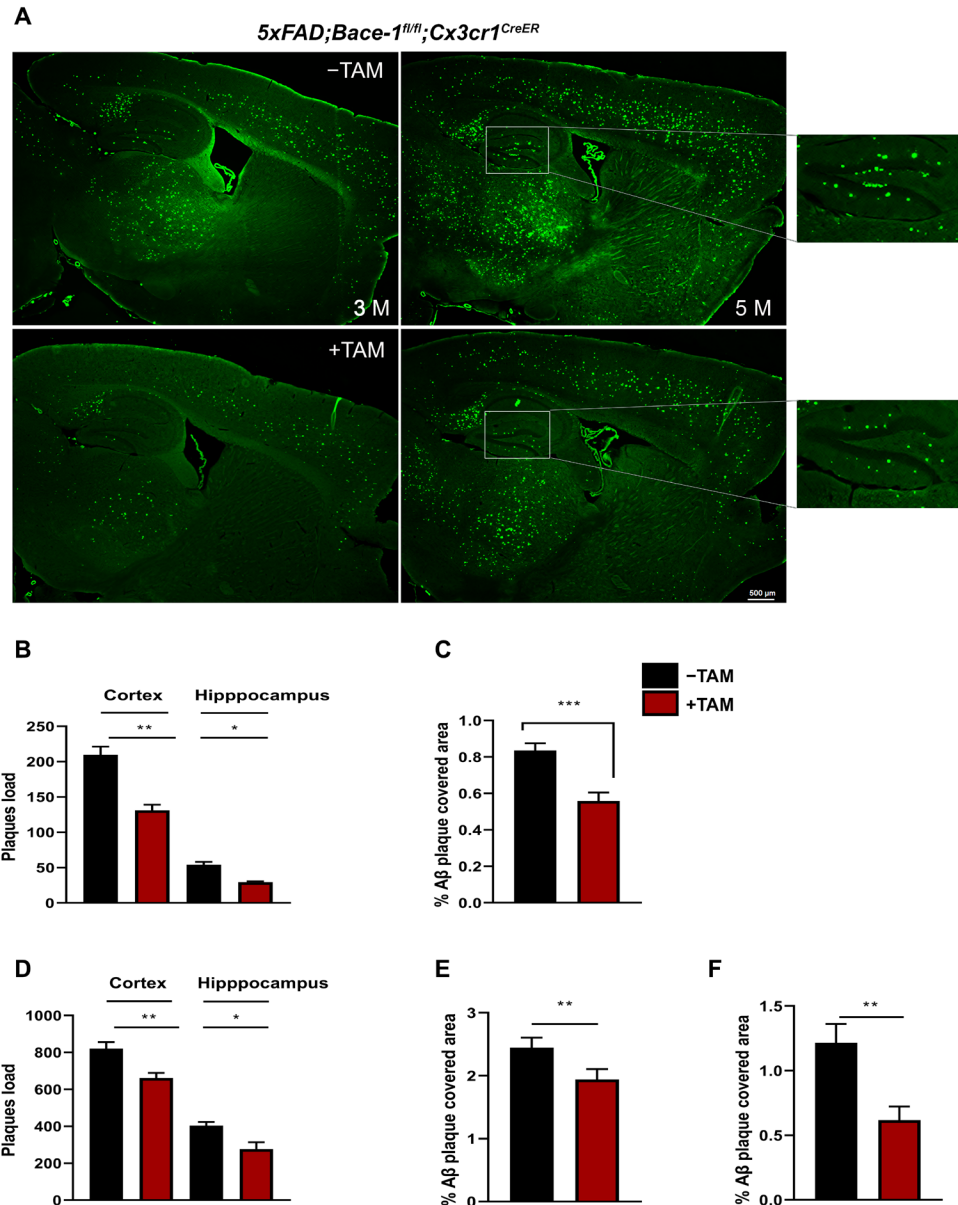


Fig. 2. Targeted Bace-1 deletion in microglia decreases amyloid plaques in 5xFAD mice. (A) Bace-1 was deleted in microglia by using Bace-1 conditional knockout mice (*Bace-1*^{f/f}) and specific expression of Cre-recombinase in microglia in *Cx3cr1*^{CreER} mice. Representative images of thioflavin S staining in 3-month-old (3 M) and 5-month-old (5 M) cerebral cortex of *5xFAD;Bace-1*^{f/f};Cx3cr1^{CreER} (+TAM) and age-matched control (no Bace-1 deletion) littermates (-TAM). Insets were enlarged from hippocampal areas; Scale bar, 500 μ m. (B and C) Quantification of thioflavin S-labeled plaques [average number per section in (B) and percentage of area covered by plaques (C) in 3-month-old *5xFAD;Bace-1*^{f/f};Cx3cr1^{CreER} (-TAM) and *5xFAD;Bace-1*^{f/f};Cx3cr1^{CreER} (+TAM) mouse brains] ($N = 5$ to 6 mice, four fields counted every 10th section per mouse; *** $P < 0.01$, two-tailed unpaired t test). Quantification of thioflavin S plaque numbers (D) and area covered (E and F) by plaques in the cerebral cortex and hippocampus of 5-month-old AD mice ($N = 5$ to 6 animals per genotype, four fields counted every 10th section per mice; * $P < 0.05$ and ** $P < 0.01$, unpaired Student's t test)

$\text{A}\beta_{1-42}$ levels at 3 and 5 months were further quantitatively measured by enzyme-linked immunosorbent assay (ELISA). Microglial *Bace-1* deletion significantly reduced insoluble $\text{A}\beta$ levels by 34 and 20% at 3 and 5 months, respectively (* $P < 0.05$ and ** $P < 0.01$; Fig. 3E). *Bace-1* deletion in microglia also decreased soluble $\text{A}\beta$ levels by 38 and 27% in these two age groups (* $P < 0.05$ and ** $P < 0.01$; Fig. 3F). Together, these data show that microglial *Bace-1* deletion decreases amyloid plaques, mainly through enhancing their clearance rather

than through reducing amyloidogenic processing of APP. The reduction in soluble $\text{A}\beta$ levels may suggest that amyloid plaques consist of both soluble and insoluble $\text{A}\beta$.

Bace-1 deletion in microglia enhances microglial contacts with amyloid plaques

Because *Bace-1* deletion in *5xFAD;Bace-1*^{f/f};Cx3cr1^{CreER} mice reduces mainly $\text{A}\beta$ levels, we asked whether activated microglia in TAM-treated

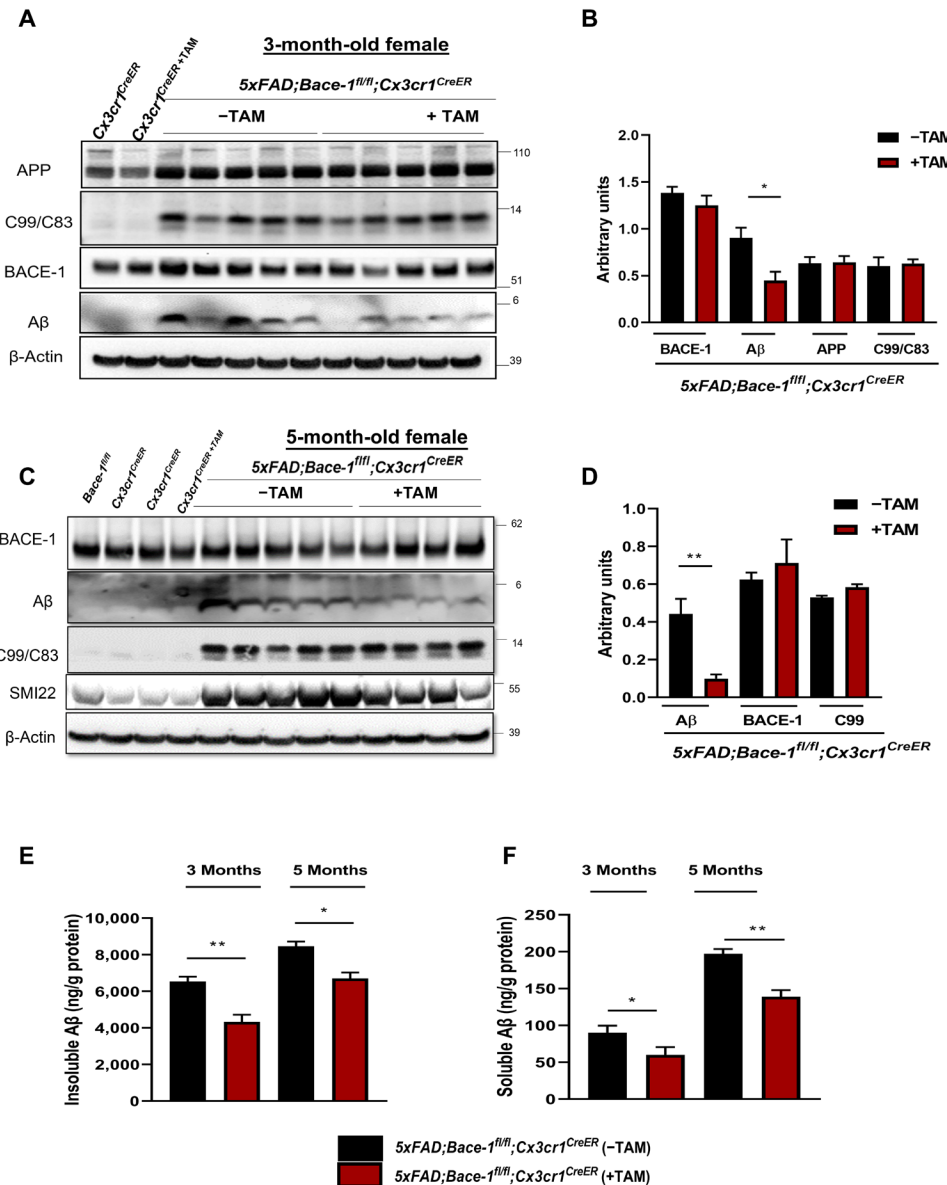


Fig. 3. Deletion of microglial Bace-1 in 5xFAD mice decreases A β levels, but not APP C99. (A and C) Hippocampal lysates from 3-month-old (A) and 5-month-old (C) female 5xFAD;Bace-1 $^{fl/fl}$;Cx3cr1 CreER (-TAM), 5xFAD;Bace-1 $^{fl/fl}$;Cx3cr1 CreER (+TAM), and control mouse brains were used to measure levels of full-length APP, C-terminal fragments (C99 and C83), BACE-1, and A β . Bar graphs in (B and D) show quantification normalized to β -actin (*P < 0.05; Student's t test, N = 5 for both genotypes). (E and F) Quantification of A β levels (soluble and insoluble) in the cerebral cortex of female mice at 3 and 5 months of age by ELISA (N = 5 to 8 per group, *P < 0.05 and **P < 0.01, unpaired Student's t test).

5xFAD;Bace-1 $^{fl/fl}$;Cx3cr1 CreER mice would be more phagocytic. To answer this, we first examined whether association of microglia with the amyloid plaque would be increased. Significantly more microglia, as labeled by IBA-1 antibody, were in close contact with amyloid plaques in TAM-treated 5xFAD;Bace-1 $^{fl/fl}$;Cx3cr1 CreER mice compared to control littermates (Fig. 4A). Quantification of microglial cells per plaque showed a significantly greater number in TAM-treated 5xFAD;Bace-1 $^{fl/fl}$;Cx3cr1 CreER mice compared to control littermates (30 ± 0.11 versus 3.2 ± 0.10; Figs. 4B and 2), although the size of amyloid plaques was visibly smaller in Bace-1-deleted 5xFAD;Bace-1 $^{fl/fl}$;Cx3cr1 CreER mice compared to control littermates. Bace-1 deletion also induced a unique phenotypic morphology, with significantly

higher process area (201 ± 15.7 μm^2 versus 331 ± 17 μm^2 ; Fig. 4C), as well as more extensive microglial process branching patterns (94 ± 0.74 versus 10.18 ± 0.42; Figs. 4D and 5). The significantly increased colocalization with thioflavin S-positive plaques of microglia in both male (4.46 ± 0.38% versus 6.7 ± 0.7%) and female 5xFAD;Bace-1 $^{fl/fl}$ mice (1.8 ± 0.19% versus 4.9 ± 0.41%) were similarly affected (fig. S4, A to D).

Further evidence was provided by costaining of microglia using CD68 antibody and thioflavin S: More CD68 $^+$ microglia were in contact with amyloid plaques (12.02 ± 0.23 spots per plaque versus 16.0 ± 0.96 spots per plaque; Fig. 4, E and F). Hence, both biochemical and morphological data, together with results from in vitro our

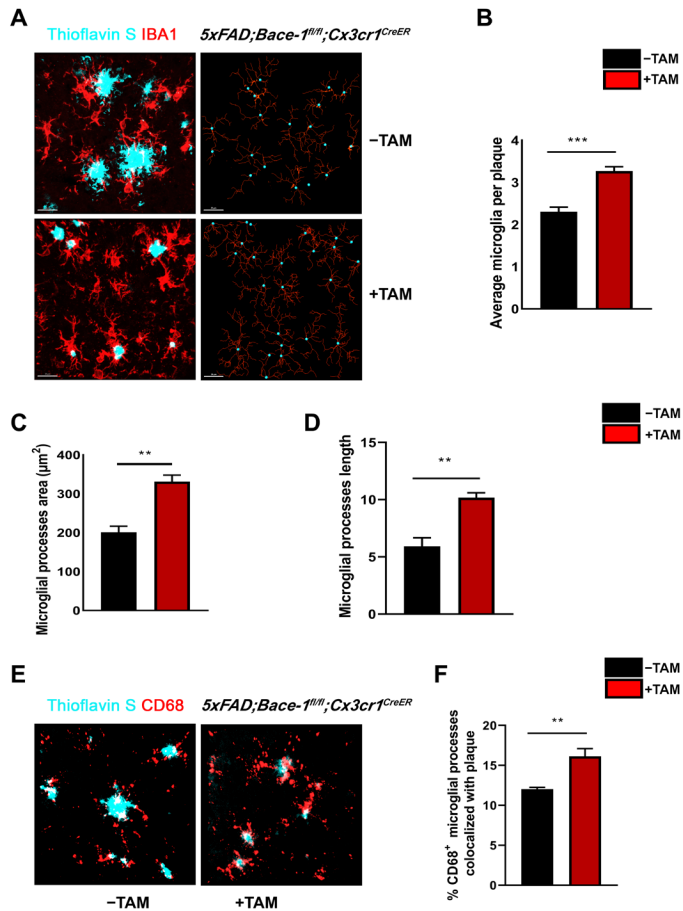


Fig. 4. Bace-1 deletion induces microglial activation in the 5xFAD mouse model. (A) Representative three-dimensional (3D) reconstruction of confocal Z-stack images from the subiculum of WT and *Bace-1*-null mice. IBA-1-positive microglia processes are shown in red, surrounding the thioflavin S-positive amyloid plaques in green. Increased engulfment of amyloid is appreciable in *Bace-1*-deleted microglia compared to *5xFAD;Bace-1^{f/f};Cx3cr1^{CreER}* (-TAM). Scale bars, 20 μ m. (B) Quantification of the number of plaque-associated microglia ($N = 3$ pairs of mice, 100 plaques randomly selected per genotype; *** $P < 0.001$, Student's *t* test). (C and D) Imaris software-based quantification of microglial parameters expressed as averaged volume area and process lengths and represented as means \pm SEM ($N = 3$, animals per genotype). *Bace-1* deletion enhances microglial infiltration and cross-talk with A β plaques. (E) Representative 3D reconstruction of confocal Z-stack images from the subiculum of WT and *Bace-1*-null mice. CD68-positive immune cells are labeled in red, surrounding and overlapping with the thioflavin S-positive amyloid plaques in green. Increased colocalization of CD68, a lysosomal marker with amyloid plaques, is appreciable in *Bace-1*-deleted microglia cells compared to *5xFAD;Bace-1^{f/f};Cx3cr1^{CreER}* (-TAM). (F) Quantification of the percentage of CD68 region of interest (red channel) colocalized with thioflavin S-positive amyloid plaques (green channel) presented as means \pm SEM. $n = 25$ plaques and surrounding microglia. ** $P < 0.01$.

phagocytic assays (16), support enhanced microglial phagocytic functions in response to *Bace-1* deletion in microglia.

Bace-1 deletion in microglia enhances lysosomal degradation

In our immunoblot assays, we noted a significant increase in the autophagosomal protein microtubule-associated protein 1 light chain 3 beta (LC3B) in TAM-treated *5xFAD;Bace-1^{f/f};Cx3cr1^{CreER}* mice

(fig. S3, A and B), suggesting a change in phagolysosomal function. We further conducted multiple in vitro immunoblot assays by treating primary microglia with oligomeric A β ₄₂. Again, the autophagosomal protein LC3B was consistently found to be elevated in all of the same lysates, indicating a more active autophagolysosomal function upon *Bace-1* deletion in microglia. Moreover, levels of lysosomal proteases such as cathepsin D (CTSD), CTSB, lysosomal-associated membrane protein 1 (LAMP1), and LAMP2 were also significantly elevated (Fig. 5A); changes in mRNAs coding for these proteins were not evident on the basis of single-cell RNA-seq results (16). Quantification confirmed significantly higher protease levels (Fig. 5B). Similar changes were also observed if *Bace-1* was knocked down by small interfering RNA (siRNA) in primary microglia (fig. S5, C and D).

Higher protein levels likely suggest higher lysosomal functions. We found increased CTSD proteolytic activity in both *Bace-1*-null (Fig. 5C) and *Bace-1*-siRNA knockdown microglia (fig. S5E), correlating with enhanced CTSD protein levels. When lysosomal/autophagosomal protease activity was elevated, more up-taken A β _{1–42} in BACE-1-inhibited bone marrow-derived macrophages and microglia cells were likely to be degraded. A β levels were overall lower in *Bace-1*-null microglia (Fig. 5, A and B), as they were higher at 1- to 2-hour incubation, due to more uptake initially but lowered during prolonged incubation, attributable to more effective degradation (also see data in fig. S5C).

We also showed that BV-2 cells treated with the BACE-1 inhibitor AZD-3293 displayed dose-dependent elevation of lysosomal protease levels (Fig. 5D). Quantification confirmed elevation of these lysosomal proteases (Fig. 5E) and subsequent dose-dependent A β degradation (Fig. 5F). Hence, deletion or inhibition of BACE-1 in microglia not only enhances phagocytosis but also facilitates degradation of A β , contributing to the reduced amyloid deposition seen in TAM-treated *5xFAD;Bace-1^{f/f};Cx3cr1^{CreER}* mice.

BACE-1 regulates A β -induced metabolic reprogramming in microglial cells

Both receptor-based phagocytosis and micropinocytosis involve in dynamic reorganization of the cytoskeleton. To meet the energy demands associated with A β uptake and mounting inflammatory immune responses, microglia efficiently undergo a metabolic switch from mitochondrial oxidative phosphorylation (OXPHOS) to glycolysis (18). To explore whether BACE-1 regulates A β -induced metabolic reprogramming, we compared the mitochondrial bioenergetics profiles by monitoring changes in the oxygen consumption rate (OCR), which is an indicator for OXPHOS. As shown in Fig. 6 (A and B), while the OCR levels were comparable, *Bace-1* deletion induced a significant alteration in extracellular acidification rate (ECAR) levels, which is an indicator of glycolysis. WT microglia responded to A β challenge by inducing an increase in ECAR levels by ~11%, while *Bace-1* deletion significantly increased ECAR levels by ~25% (** $P < 0.01$; Fig. 6B). Furthermore, in comparison to A β -treated WT microglia, *Bace-1* deletion increased glycolysis by ~42% ($N = 9$, *** $P < 0.001$; fig. S6).

To determine the maximal respiration capacity that cells can attain under stress conditions, carbonyl cyanide *p*-trifluoromethoxyphenylhydrazone (FCCP), an uncoupler of mitochondrial electron transport chain, was added to stimulate the oxygen consumption necessary for maintaining the proton gradient across intermitochondrial membranes. As shown in Fig. 6D, maximal respiration was maintained in WT microglia; however, *Bace-1* deletion enhanced the maximal respiration capacity by ~17%. To further measure the

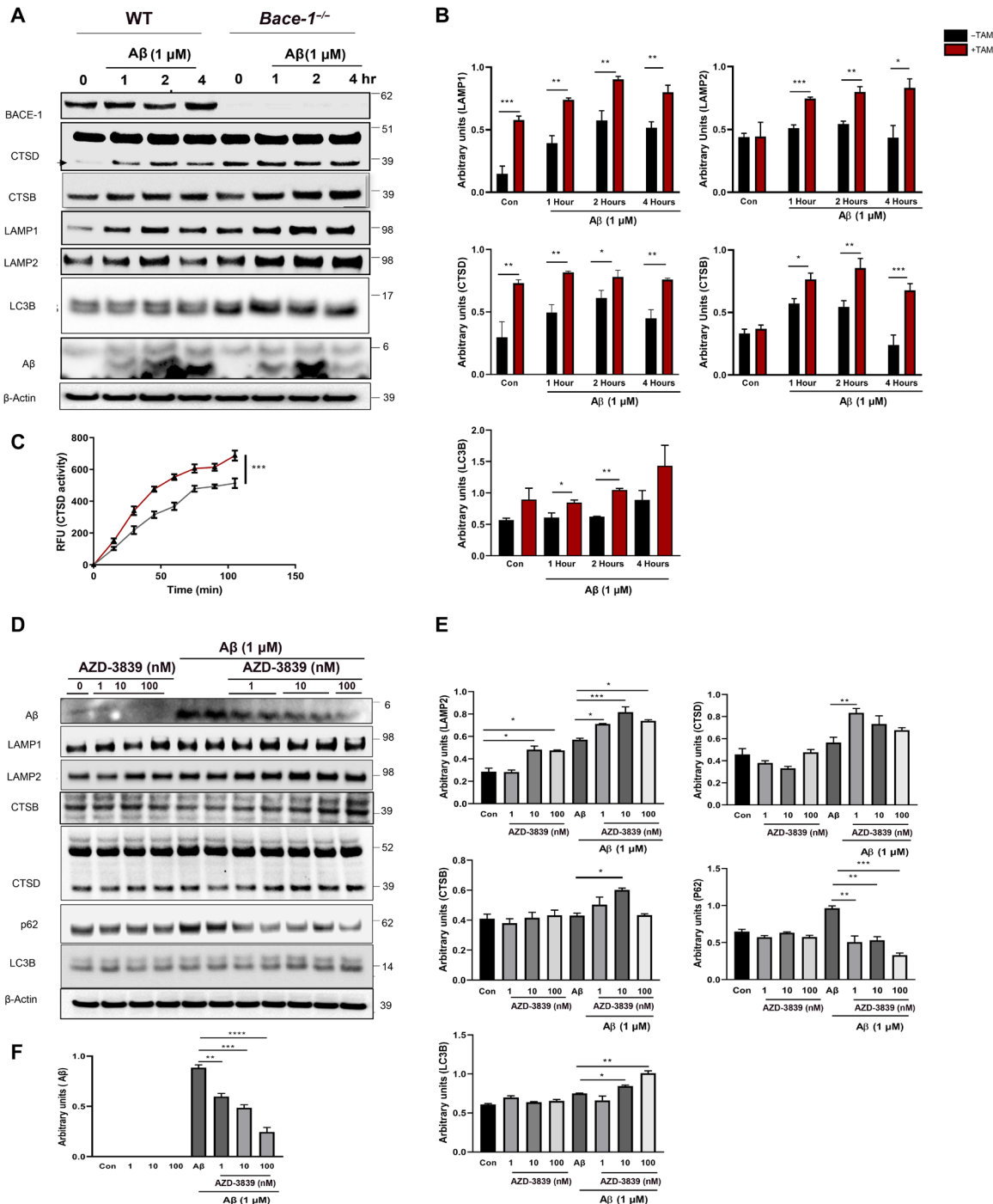


Fig. 5. *Bace-1* deletion in microglia enhances degradation of phagocytosed A β . (A) Autophagic and lysosomal proteases such as CTSD (marked by arrow), CTSB, and LAMP1 and LAMP2, and LC3B were examined using lysates from WT and *Bace-1*-null primary microglia with or without A β treatment for the indicated time intervals. (B) Quantification of immunoblots is shown in the bar graphs, with data from at least three independent experiments (*P < 0.05 and **P < 0.01, Student's t test). (C) CTSD activity (kinetics) was measured every 10 min over a period of 2 hours after A β treatment in WT and *Bace-1*-null microglia (N = 6; *P < 0.05 and **P < 0.01, Student's t test). (D to F) Autophagy lysosomal protein degradation was examined using lysates from BV-2 pretreated with the BACE-1 inhibitor AZD-3839 (1, 10, or 100 nM), followed by A β_{1-42} treatment for 5 hours. Quantification is shown in the bar graphs in (E). Increased degradation of phagocytosed A β_{1-42} , represented from (D), is shown in (F). *P < 0.05, **P < 0.01, or ***P < 0.001, Student's t test.

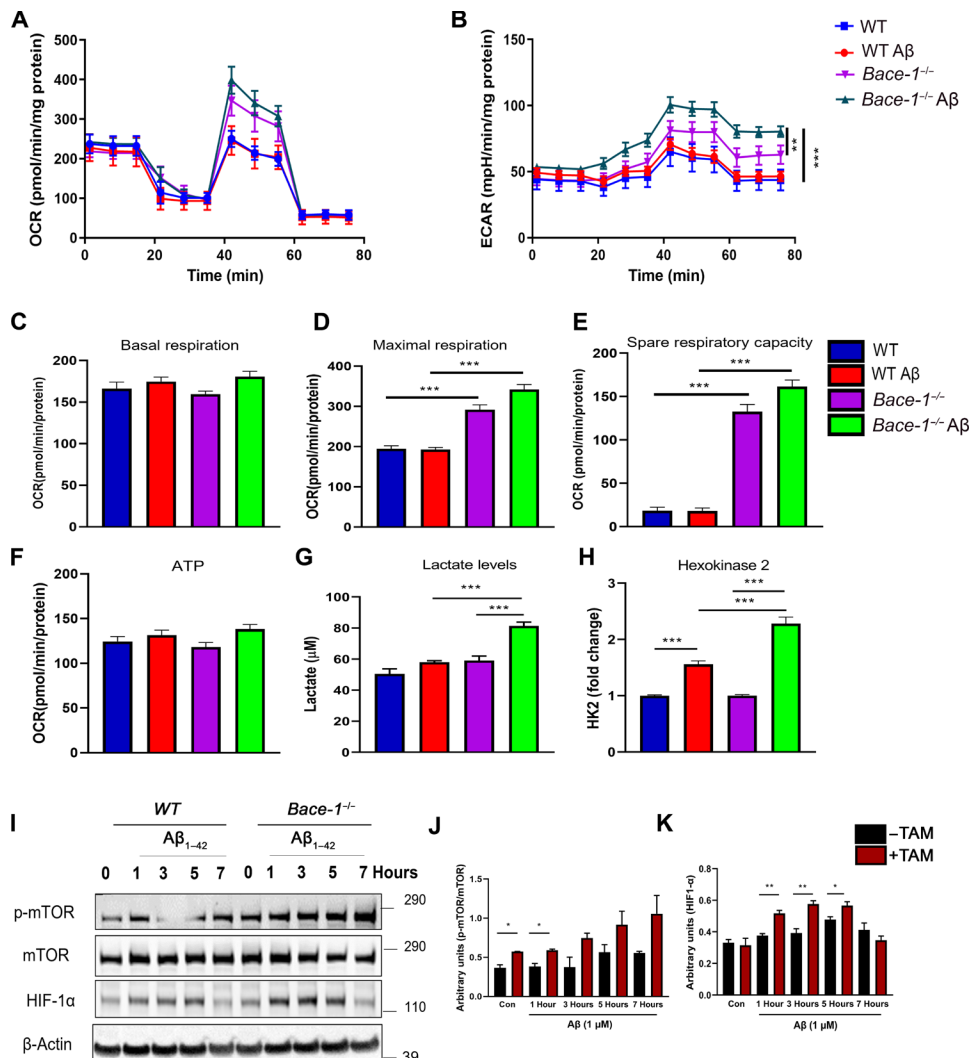


Fig. 6. Bace-1 deletion markedly induces A β -induced glycolysis in microglia. WT and Bace-1-null microglia were treated with and without A β for 3 hours. After treatment, real-time changes in OCR/ECAR levels were determined following sequential addition of mitochondrial stressors oligomycin, FCCP, and rotenone and antimycin as illustrated. Schematic representation of OCR, (A) ECAR, a glycolytic indicator (B), basal (C), maximum respiration (D), spare respiratory capacity (E), and ATP (F) as calculated using Seahorse Wave software. Data were normalized per milligram protein and are presented as means \pm SEM. N = 9. *P < 0.05, **P < 0.01, and ***P < 0.001, two-way ANOVA. Data are representative of one of the two independent experiments. (G) Lactate levels in the supernatant of WT and Bace-1-null BV-2-treated cells with and without A β for 12 hours. Data were normalized per milligram protein and are presented as means \pm SEM. N = 8. ***P < 0.001, Student's t test. Data are representative of one of the three independent experiments. (H) HK2 gene expression in WT and Bace-1-null microglia treated with A β for 12 hours. Bulk RNA-seq was conducted to determine the microglial transcriptomic profile. Data are presented as fold change normalized to respective controls. N = 3. ***P < 0.001, Student's t test. (I) Immunoblot analysis of mTOR, phosphorylated mTOR (p-mTOR), HIF-1 α , and β -actin in WT and Bace-1-null microglia treated with and without A β 1-42 for various time points. (J and K) Quantification data are presented as means \pm SEM. *P < 0.05, Student's t test.

ability of microglia to cope with increasing energetic demands, cells were treated with rotenone/antimycin A, and spare reserve capacity was quantified. A β treatment led to a marked reduction (~36%) in spare respiratory capacity in WT microglia, while in Bace-1-deleted microglia, it enhanced the spare capacity by ~22% (Fig. 6E), indicating that BACE-1 deficiency mitigates A β -induced mitochondrial bioenergetic deficits in microglia.

We further quantified OXPHOS-linked adenosine 5'-triphosphate (ATP) levels in both WT and Bace-1-null microglia. Bace-1-null cells, after A β treatment, increased ATP production by ~17%, while WT cells had a marginal increase in ATP levels (~5%; Fig. 6F).

suggesting that during early hours of phagocytosis and A β clearance, microglia draw energy mainly from glycolytic pathways and, to some extent, from OXPHOS. Because lactate is the end product of glycolysis, we measured changes in lactate levels after A β treatment. Bace-1 deletion significantly enhanced A β -induced glycolysis (58.01 ± 0.97 versus 81.36 ± 2.4 , ***P < 0.001; Fig. 6G) in the microglial cells, confirming that BACE-1 deficiency unlocks the energy necessary via glycolysis for mounting a robust immune response aimed at both A β uptake and clearance.

We then examined whether this enhanced glycolysis would be associated with A β -induced changes in the gene expression profiles.

Hexokinase-2 (HK2) is a critical enzyme that initiates the first steps of glycolysis by catalyzing phosphorylation and diverting D-glucose-6-phosphate into the glycolytic pathway (19). Intriguingly, *Bace-1* deletion induced a ~2.4-fold increase in the HK2 gene as compared to a ~1.55-fold induction in A β -treated WT microglia (Fig. 6H).

The phosphatidylinositol 3-kinase (PI3K)-mammalian target of rapamycin complex (mTOR) pathway regulates glycolysis by inducing hypoxia-inducible factor-1 α (HIF-1 α) signaling. Previously, we demonstrated significant up-regulation of PI3K-AKT signaling in BACE-1-deficient microglia after A β treatment (16). We therefore examined whether BACE-1 modulates glycolysis by regulating the PI3K-mTOR-HIF-1 α signaling pathways. Primary microglia from WT and *Bace-1*-null mixed glial cultures were treated with A β for various time points. Immunoblot analyses showed that *Bace-1* deletion significantly enhanced A β -induced phosphorylation of mTOR at Ser²⁴⁴⁸, as well as downstream HIF-1 α as early as 1 hour after A β treatment (Fig. 6I). Further quantification was shown in Fig. 6J and K (*P < 0.05 and **P < 0.01). In addition, *Bace-1* deletion induced a ~3.1-fold increase in the HIF-1 α gene as compared to a ~2.56-fold induction in A β -treated WT microglia (fig. S6B). Together, our study indicates that BACE-1 is not merely limited to neuronal APP processing, but it also regulates immune responses by modulating cellular metabolism during acute inflammatory conditions.

***Bace-1* deletion in microglia improves learning and memory behaviors in 5xFAD mice**

Because a high load of A β deposition is associated with synaptic loss and memory deficits (20), we asked whether the significant reduction in A β after microglial *Bace-1* deletion rescued A β -mediated impairments in hippocampal-dependent memory tasks. The Y-maze exploratory task, which relies heavily on hippocampal-dependent spatial working memory function, was first performed to measure changes in spontaneous alternations. While the average numbers of total entrances in the three arms were similar among the different mouse groups (Fig. 7A), TAM-treated 5xFAD; *Bace-1*^{f/f}; *Cx3cr1*^{CreER} mice at the age of 6 to 7 months exhibited significantly higher spontaneous alternations (48 ± 1.8%) compared to 5xFAD; *Bace-1*^{f/f}; *Cx3cr1*^{CreER} mice treated with only corn oil (40 ± 1.4%; **P < 0.01; Fig. 7B). This indicates that BACE-1 deficiency in microglia partially restored impaired spatial working memory.

We further tested hippocampus-dependent memory-related tasks by performing the standard contextual fear conditioning test, similar to our previous study (8). Contextual fear memory was measured by scoring freezing behaviors. On day one, which is mostly for preconditioning purposes, mice were placed in the fear conditioning chamber for 3 min, exposed to a sound stimulus for two 30-s intervals, followed by a foot shock. There were no statistically significant differences among the different genotypes of mice in terms of percentage of freezing time in either the pre- or posttone period. On the second day of context-based memory, TAM-treated 5xFAD; *Bace-1*^{f/f}; *Cx3cr1*^{CreER} mice showed a higher percentage of freezing time (37.5 ± 3.3%) than nondeleted control 5xFAD; *Bace-1*^{f/f}; *Cx3cr1*^{CreER} mice (26.8 ± 2.5%), closer to the control groups (47.7 ± 3.7% in *Bace-1*^{f/f} mice versus 40.3 ± 3.2% in *Bace-1*^{f/f}; *Cx3cr1*^{CreER} mice in Fig. 7C; *P < 0.05 and ***P < 0.001). This result also suggests that removal of amyloid plaques improves performance in the contextual fear conditioning test. On day 3 of the cue test, the freezing time in TAM-treated 5xFAD; *Bace-1*^{f/f}; *Cx3cr1*^{CreER} mice was also significantly

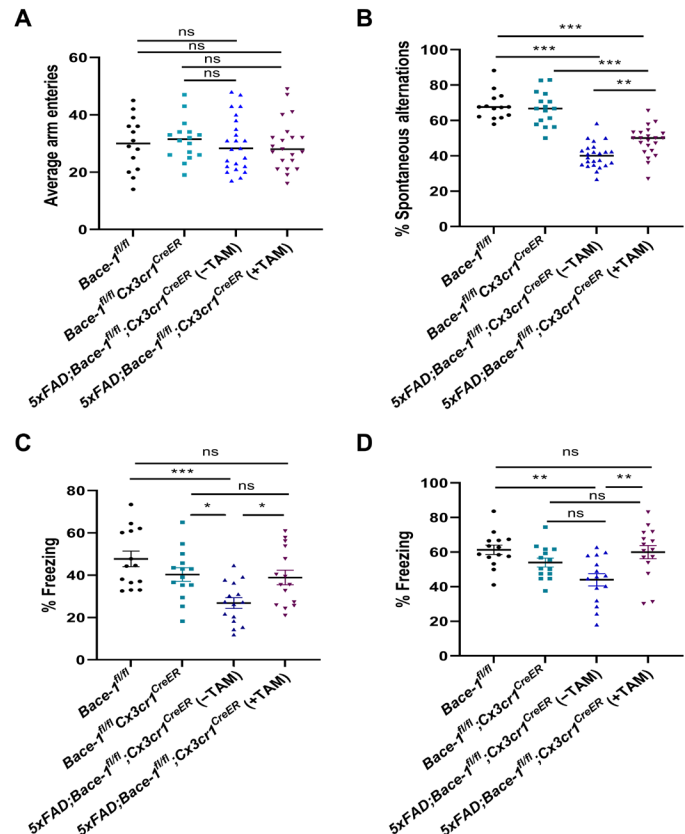


Fig. 7. Targeted BACE-1 inhibition in microglia markedly rescued behavioral and long-term potentiation deficits in the 5xFAD mice model. (A and B) Y-maze tests were performed in 6- to 7-month-old *Bace-1*^{f/f}, *Bace-1*^{f/f}; *Cx3cr1*^{CreER}, and 5xFAD; *Bace-1*^{f/f}; *Cx3cr1*^{CreER} mice. Tamoxifen treatment induced expression of Cre recombinase to delete *Bace-1* in microglia. Average arm entries were comparable among all groups, while *Bace-1* deletion reverted the reduction in spontaneous alternations seen in 5xFAD (non-TAM-treated 5xFAD; *Bace-1*^{f/f}; *Cx3cr1*^{CreER}) mice ($n = 22$; **P < 0.01 and ***P < 0.001, one-way ANOVA). (C and D) A standard fear conditioning test was performed to assess hippocampal-dependent contextual and cue memory. Impairments in contextual fear conditioning on day 2 were observed in nontreated 5xFAD; *Bace-1*^{f/f}; *Cx3cr1*^{CreER} mice, and *Bace-1* deletion after TAM treatment reverted these impairments as evidenced by increased contextual freezing on the second day (C). Similarly, impaired contextual experiences on day 3 were also reverted by *Bace-1* deletion [(D) $n = 14$ to 16 mice per group; *P < 0.05, **P < 0.01, or ***P < 0.001, one way-ANOVA]. ns, not significant.

reduced compared to control littermates (59.9 ± 3.8% versus 44.0 ± 3.5% in Fig. 7D; **P < 0.01). Hence, reduced amyloid deposition can improve learning behaviors.

Deletion of *Bace-1* only in microglia improves synaptic function in the 5xFAD mouse model

We further examined whether the significant reduction in A β also rescued hippocampal synaptic plasticity by measuring long-term potentiation (LTP) in the Schaffer collateral pathway, as induced with high-frequency stimulation. As shown in Fig. 8 (A and B), 8-month-old 5xFAD mice (oil-treated 5xFAD; *Bace-1*^{f/f}; *Cx3cr1*^{CreER} mice) exhibited reduced LTP, but this reduction was reverted in TAM-treated 5xFAD; *Bace-1*^{f/f}; *Cx3cr1*^{CreER} mice (163.2 ± 3.790 in -TAM versus 189.3 ± 5.159 in +TAM; 228.4 ± 16.00 in WT mice; N = 10, ***P < 0.001, Student's t test; Fig. 8A). Hence, electrophysiological

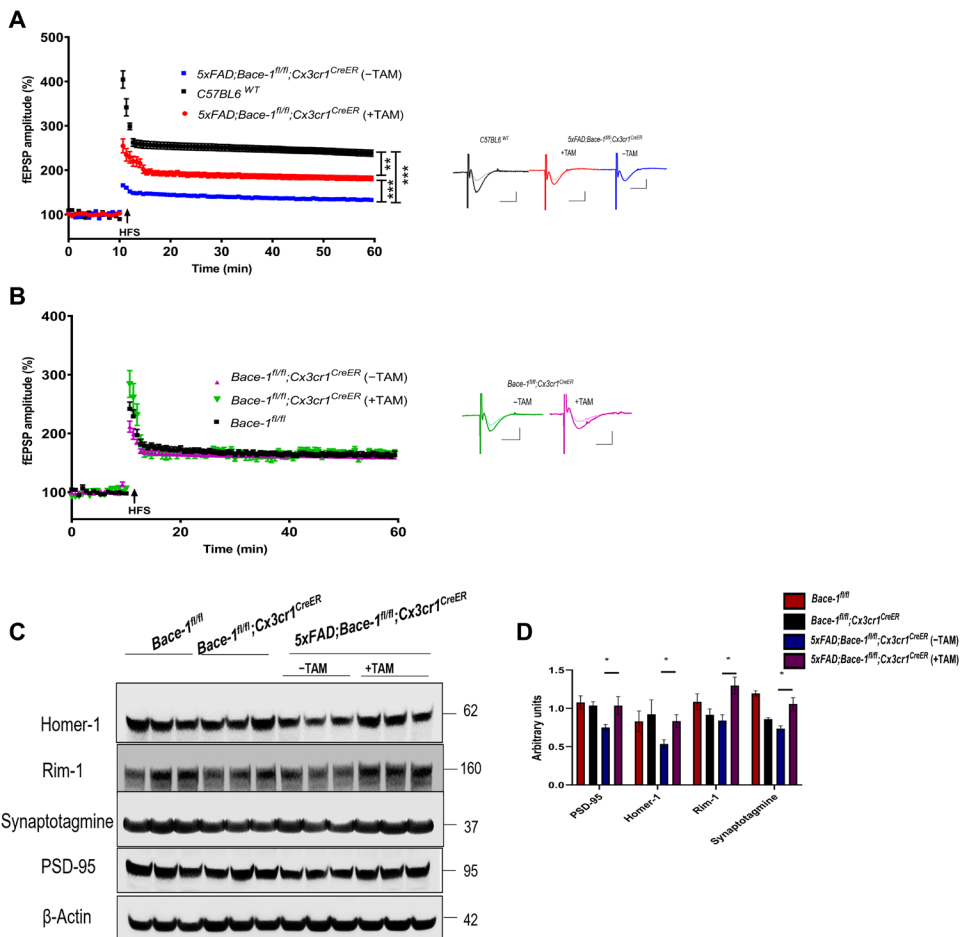


Fig. 8. Targeted Bace-1 inhibition in microglia markedly rescued behavioral and long-term potentiation deficits in the 5xFAD mice model. (A) LTP was recorded on horizontal hippocampal slices from 6-month-old 5xFAD;Bace-1^{f/f};Cx3cr1^{CreER} mice with or without TAM treatment beginning at 2 months age. Time course of fEPSP recorded and plotted every minute in the hippocampal CA1 region before and after 100-Hz stimulation (60 min) in the Schaffer collateral region. The colored example traces matched with the LTP fEPSP plot. N = 10 slices from five mice per group; **P < 0.01, ***P < 0.001, Student's t test. (B) LTP was also compared in non-AD Bace-1^{f/f};Cx3cr1^{CreER} mice with (+TAM) or without (-TAM) deleting Bace-1 in microglia. BACE-1 deletion in microglia preserved synaptic function in the 5xFAD mice model. HFS, high-frequency stimulation. (C) Synaptic proteins from the cortex and hippocampus of 8-month-old mice were analyzed by immunoblotting for various presynaptic and postsynaptic markers. (D) Quantification of immunoblots are presented as means ± SEM (N = 3, *P < 0.05; Student's t test).

experiments support ameliorated synaptic function upon *Bace-1* deletion in microglia, due largely to enhanced clearance of amyloid plaques.

We and others have previously demonstrated that *Bace-1* deletion or inhibition in adult AD mice causes impairments in synaptic function, reflected by reduced LTP, and that this impairment is likely due to abolished cleavages of BACE-1 substrates in neurons. This is consistent with the failure of BACE-1 inhibitors in clinical trials, which showed impaired cognitive functions in individuals taking BACE-1 inhibitors. To determine whether inhibition or deletion of *Bace-1* in microglia would affect synaptic functions, we conducted LTP measurements in *Bace-1*^{f/f};Cx3cr1^{CreER} mice with TAM treatment. We found that deletion of *Bace-1* in microglia had comparable LTP to control littermates (Fig. 8B). This finding is particularly significant because targeted deletion of BACE-1 in microglia shows no impairments in synaptic functions, unlike LTP reduction seen in mice with broad deletion of *Bace-1* as previously reported (8).

Because enhanced microglia-mediated Aβ clearance improved synaptic functions in 5xFAD mice, we compared levels of several pre- and postsynaptic proteins in the synaptosome-enriched samples at 8 to 9 months of age. While in non-TAM *Bace-1*^{f/f};Cx3cr1^{CreER} mice, there were significant reductions in both presynaptic (Rim-1 and synaptotagmine) and postsynaptic [postsynaptic density protein 95 (PSD-95) and Homer-1] markers without TAM treatment, but *Bace-1* deletion in microglial cells reversed the reductions in these synaptic proteins (*P < 0.5; Fig. 8, C and D), which is consistent with the results from our LTP assays. Together, our results suggest that enhancing microglial-mediated Aβ clearance preserved synaptic functions.

DISCUSSION

AD is an age-dependent progressive neurodegenerative disease impairing cognitive functions, presumably resulting from age-dependent excessive Aβ buildup in the brain along with defective clearance. This hypothesis is supported by genetic and epidemiologic studies (21–23).

Inhibition of BACE-1 to reduce A β generation and amyloid plaques has emerged as one of the most important therapeutic approaches for treating patients with AD (4, 24). However, inhibition of BACE-1 alone has failed to improve cognitive functions in patients with AD, indicating a need to revisit and optimize this therapeutic strategy. In this study, we have found that genetic deletion of microglial *Bace-1* in mice, or pharmacological inhibition of BACE-1 in microglial cells, not only enhances phagocytosis of aggregated A β but also degrades A β more effectively due to the increased lysosomal/autophagosomal machinery. Inhibition of microglial BACE-1 appears to spare the synaptic deficits resulting from global inhibition of BACE-1 in vivo. Our data suggest that targeted inhibition of microglial BACE-1 is a superior AD treatment option compared to global BACE-1 inhibition. This is consistent with the notion that the role of microglia in AD pathogenesis is important and indispensable, as multiple AD risk genes, including *TREM2* and *CD33*, are predominantly expressed by microglia (25–28).

Global inhibition BACE-1 will benefit patients with AD by reducing the abnormal accumulation of A β and amyloid deposition, as shown in both preclinical and clinical studies (3, 13). However, this approach has failed to improve cognitive functions in clinical trials but rather causes severe hippocampal atrophy as exhibited by reduced hippocampal volumes (29). This side effect is in line with studies in mice using either deletion or pharmacological inhibition of BACE-1, which show disorganization of the hippocampal mossy fiber infrapyramidal bundle (7) and impairments in synaptic functions (30). By using selective deletion of *Bace-1* in microglia, it will circumvent the side effects associated with such synaptic impairments that result from abrogated or inhibited cleavages of BACE-1 neuronal substrates such as neuregulin-1 (NRG1), neural cell adhesion protein close homolog of L1 (CHL1), and seizure protein 6 (SEZ6), which are known to control synaptic functions (31).

Specific deletion or inhibition of BACE-1 in microglia exhibits beneficial effects. We have recently showed that *Bace-1* deletion in microglia enhances transition of more homeostatic microglia to DAM-1 in 5xFAD brains (16). In AD brains, homeostatic microglia respond to the excessive A β buildup by switching to activated DAM-1, which is morphologically detectable in contacting A β plaques (32–34). We observed elevated DAM-1 population in 5xFAD; *Bace-1*^{fl/fl}; *UbcCreER* mice compared to nondeleted 5xFAD; *Bace-1*^{fl/fl} mice, and this elevation may promote microglia to remove more amyloid plaques. Amyloid plaques were essentially much less in 10-month-old 5xFAD; *Bace-1*^{fl/fl}; *UbcCreER* mice than in 4-month-old 5xFAD; *Bace-1*^{fl/fl}; *UbcCreER* mice [see figure 5A in (8)]. In line with results in 5xFAD; *Bace-1*^{fl/fl}; *UbcCreER* mice, mice with deletion of *Bace-1* only in microglia developed much less amyloid plaques compared to non-deleted controls (Fig. 2). This reduced amyloid deposition was not due to changes in APP processing by BACE-1, (Fig. 3) but rather due to enhanced clearance and degradation of A β (Figs. 4 and 5).

We have recently demonstrated that *Bace-1* deletion in mouse microglia leads to enhanced signaling pathways associated with phagocytosis (16). Among these pathways, PI3K-AKT signaling pathway was significantly elevated upon BACE-1 inhibition or deletion, likely due to the elevated signaling activities initiated from interleukin-1, Toll-like receptor 2 (TLR2), and TLR4. This increase will, in turn, enhance metabolic reprogramming, evidenced by significantly elevated ECAR, OCR, and spare respiratory capacity (Fig. 6). Our results are in line with a recent study, which shows metabolic reprogramming from OXPHOS to glycolysis via A β induces microglia activation

(18). It is expected that enhanced mitochondria bioenergetics supports more effective degradation of engulfed amyloid plaques (Fig. 6). We noted that *Bace-1* deletion in TAM-treated *Bace-1*^{fl/fl}; *Cx3cr1*^{CreER} mice would increase microglia in association with amyloid plaques (Fig. 4A): Amyloid plaques were significantly smaller in size, while the morphology of microglia was visibly more ramified. *Bace-1* deletion in TAM-treated *Bace-1*^{fl/fl}; *Cx3cr1*^{CreER} mice elevates protein levels of several proteases, which are important for lysosomal functions and phagosomal maturation. For example, in cultured microglial cells, *Bace-1* deletion or inhibition increased protein levels of CTSB, CTSD, LAMP1, and LAMP2 (Fig. 5A), implying higher protease activity in lysosomes. In addition, phagocytic proteins such as LC3B and sequestosome-1 (p62) were also elevated when BACE-1 is inhibited or deleted (Fig. 5, C and D), suggesting increased autophagosomal functions. How BACE-1 inhibition or deletion will increase these protease levels remain to be investigated, likely related to more phagocytic microglia signatures. Nevertheless, these *in vitro* results may partially explain why A β and amyloid plaques are reduced when microglia *Bace-1* is deleted in 5xFAD mice.

Last, an encouraging observation is the spared side effects associated with synaptic impairments following global deletion or inhibition of BACE-1. BACE-1 cleaves many important neuronal proteins such NRG-1, CHL1, SEZ6, and jagged canonical notch ligand 1 (JAG1), and abolished cleavage of these substrates usually decreases their normal signaling function, as reflected in *Bace-1*-null mice, exhibiting phenotypes such as hypomyelination, spontaneous seizures, decreased neurogenesis, and reduced LTP (35). Expression of these molecules is not detectable in microglia (based on our RNA-seq results), and the effects of these molecules in microglia are minimally affected. Deletion of microglial *Bace-1* in the WT condition showed no significant effect on LTP (Fig. 8B). Microglia have been shown to regulate synaptic plasticity in multiple ways (36). We found that the reduced synaptic protein levels in 5xFAD mice were partially reversed when microglial *Bace-1* was deleted (Fig. 8, C and D). Hence, selective deletion of *Bace-1* in microglia generates less concerns of cognitive side effects.

In summary, the present study provides compelling evidence that previously unidentified microglial BACE-1 is an improved selective therapeutic target that fine-tunes and activates microglial functions necessary for A β clearance. Decreased BACE-1 in microglia preserves synaptic functions and does not negatively affect memory behaviors in mice. Drug discovery efforts in the near future should include targeting specific BACE-1 inhibition in microglia for treating patients with AD.

MATERIALS AND METHODS

Cell culture

The immortalized BV-2 microglial cell line and primary microglia were grown in RPMI 1640 and Dulbecco's modified Eagle's medium (DMEM)-F12 medium, respectively, containing 10% fetal bovine serum, 2 mM L-glutamine, 50 U of penicillin, and streptomycin (50 μ g/ml). Cells were grown in a humidified atmosphere of 5% CO₂ at 37°C. The cells were then monitored for growth, and the medium was replaced at least every 2 days.

Primary microglial culture and isolation

Primary mixed neuroglia cultures were prepared from postnatal (P1 and P2) mouse pups as described previously (37). Briefly, meninges and blood vessels were removed from the cortex. Brain

tissues were gently triturated, and a single-cell suspension was cultured in a poly-D lysine-coated T75 flask in DMEM-F12 containing 10% heat-inactivated fetal bovine serum, 2 mM L-glutamine, and 1% penicillin/streptomycin (Life Technologies) for 12 to 14 days. Microglia were separated from mixed glial cell cultures using either a shake-off method (180 rpm for 2 hours) or via a magnetic separation kit (EasyStep Mouse Cd11b-positive selection kit) from STEMCELL Technologies.

Preparation of fibrillar and soluble A β peptides

Peptides were solubilized in 0.1% NH₄OH containing 0.01% (w/v) NaN₃ and further resuspended in sodium phosphate buffer (pH 7.4). Peptides were oligomerized by incubation with constant rotation for 1 to 7 days at 37°C using an Innova 40 incubator shaker (New Brunswick). To ensure the presence of predominantly monomeric form, lyophilized fluorescence peptides were suspended in 0.01% NH₄OH. These solutions were stored at -20°C. Each aliquot was thawed only once immediately before the experiment.

Immunohistochemistry

Mice were anesthetized, followed by transcardial perfusion with phosphate-buffered saline (PBS) for 5 min. Brains were surgically removed and fixed in 4% paraformaldehyde for 24 hours. Brains were then cryoprotected by incubating overnight in 20% sucrose solution and embedded in optimal cutting temperature (OCT). Brains were sectioned sagittally (14 to 16 μ m thick) on a freezing microtome (MICROM GmbH). Sections on the slides were washed in PBS 3 \times for 5 min to remove OCT and then permeabilized with 0.5% Triton X-100 for 30 min, followed by washing with PBS (3 \times for 5 mins). Antigen retrieval was performed by microwaving the sections in 0.05 M citrate-buffered saline (pH 6.0) for 2 min. The sections were blocked with 4% normal goat serum and 1% bovine serum albumin (BSA) and incubated overnight at 4°C with primary antibodies at the following dilutions: 6E10 (1:1000), IBA1 (1:1000), BACE-1 (1:250; AB_2313859, Covance), and A β 1-42 (1:500; AB_2341375, IBL-American). After incubation, sections were washed with PBS (4 \times for 5 min), followed by counterstaining with Alexa Fluor-conjugated secondary antibody (1:500 in blocking buffer) at room temperature (RT) for 2 hours. After additional PBS washes (4 \times for 5 min), Hoechst 33342 (final concentration of 10 μ g/ml in PBS) was added to stain the nuclei at RT for 8 min. Thioflavin S-positive A β plaques were detected by incubating sections in thioflavin S for 15 min. Slides were washed twice in PBS and mounted on a coverslip with Antifade mounting medium. Images were captured with either a Keyence fluorescence microscope or a Zeiss LSM 800 confocal microscope.

CTSD activity assay

Caspase activity was measured using a commercially available CTSD assay kit (catalog no. K143-100). Briefly, BV-2 cells (1×10^6 per well) were grown on six-well plates. After A β treatment completion, cells were washed twice in ice-cold PBS and lysed in cell lysis tris buffer [50 mM tris-HCl (pH 7.4), 1 mM EDTA, 10 mM EGTA, and 10 μ M digitonin] for 10 to 15 min on ice. Lysates were centrifuged at 10,000g for 5 min, and the resulting supernatants were incubated with an equal volume of reaction buffer containing specific fluorogenic CTSD substrate [GKPILFFRLK(Dnp)-D- R-NH₂] labeled with MCA and incubated at 37°C for 1 hour. Caspase activity (cleaved substrate) was measured using the SpectraMax microplate reader with an excitation wavelength of 328 nm and an emission wavelength of

460 nm. Caspase activity was expressed as fluorescence units per milligram protein.

A β detection

Enzyme-linked immunosorbent assay

Mice were anesthetized with isoflurane and perfused with PBS (pH 7.4). The brains were extracted, and cortices and hippocampi were dissected. To assess A β levels, mouse cortical brain tissue (frontal cortex) was homogenized in 5 \times volumes of tris-buffered saline (TBS) containing 5 mM EDTA and 1:100 protein phosphatase inhibitor (Roche). The homogenate was centrifuged at 100,000g for 20 min at 4°C. Supernatants were collected and analyzed for TBS-soluble A β fraction. The resultant pellet was resuspended in 5 \times 5 M guanidine and 50 mM tris (pH 8). The homogenate was allowed to spin in the rotor overnight. Samples were resuspended in 1:10 loading buffer (PBS, 0.05% Tween 20, and 1% BSA) and centrifuged at 100,000g for 10 min at 4°C, and supernatants were collected for insoluble A β analysis. Both soluble and insoluble A β were quantified for A β ₁₋₄₂ via an ELISA-based immune assay.

Assessment of A β plaque burden in mice

Sagittal sections were stained with the thioflavin S (0.01%). Every 10th section from the beginning of the hippocampus was stained and counted for A β plaques. The amyloid plaque burden, as well as area occupied by all plaques divided by the total area of cortex and hippocampus, was estimated using ImageJ software. A total of four to five brain sections were analyzed per mouse. Data are presented as averaged means \pm SEM.

Western blotting

Post-A β or compound treatment, the BV-2 cells or microglia were washed twice with ice-cold PBS and lysed on ice in radioimmuno-precipitation assay lysis buffer containing 50 mM tris-HCl (pH 7.4), 1 mM EDTA, 100 mM NaCl, 0.1% SDS, 1 mM phenylmethylsulfonyl fluoride, 1 mM sodium orthovanadate, leupeptin (1 μ g/ml), pepstatin (1 μ g/ml), and aprotinin (10 μ g/ml) for 5 min. The lysate was collected and further sonicated on ice for 30 s on and off cycle for 5 min and then centrifuged at 15,000g for 15 min at 4°C. Protein concentrations were determined using a bicinchoninic acid (BCA) assay kit (26). Equal amounts of protein from each sample were loaded and electrophoretically resolved on 4 to 12% SDS-polyacrylamide gel electrophoresis (NuPAGE system, Life Technologies) gels. After electrophoresis, proteins were transferred to nitrocellulose membranes at 100 V for 2 hours. The membranes were blocked with 5% BSA for 1 hour at RT. The membranes were probed with primary antibody (1:1000 dilution), as listed in Table 1, followed by incubation with secondary fluorescence-labeled antibody (1:3000). The antibody-bound proteins were detected by an iBright 1500 imaging system (Invitrogen). To ensure equal loading, the blots were reprobed with monoclonal anti-actin (1:1000). For quantification purposes, band intensities of immunoblots were analyzed using ImageJ software.

LTP recordings

LTP recordings on hippocampal slices were performed according to previously described procedures using a MED-A64HE1S head amplifier and a MED-A64MD1 main amplifier, run by Mobius software (8, 30). Upon obtaining horizontal hippocampal slices from the brains of 4- to 7-month-old mice, the prepared slices were then placed onto the center of an MED probe (MED-P515A; AutoMate

Table 1. Antibodies used in the study. TREM2, triggering receptor expressed on myeloid cells 2; APOE, apolipoprotein E; RRID, Research Resource Identifiers; pMTOR, phosphorylated mammalian target of rapamycin.

Antibody name	Catalog no.	RRID:	Company
Cathepsin D (C-20) antibody	sc-6486,	AB_637896	Santa Cruz Biotechnology
Cathepsin D antibody [EPR3057Y]	ab75852	AB_1523267	Abcam
Cathepsin B (D1C7Y) XP	31718	AB_2687580	Cell Signaling Technology Inc.
P-AKT(Ser ⁴⁷³)	9271	AB_329825	Cell Signaling Technology Inc.
β-Amyloid (1–42 specific) (D9A3A)	14974	AB_2798671	Cell Signaling Technology Inc.
Anti-APP, C-terminal antibody	A8717	AB_258409	Sigma-Aldrich
APOE (F-9)	sc-390925		Santa Cruz Biotechnology
β-Amyloid 1–16, 6E10	803003	AB_2564652	BioLegend
TREM2	ab86491	AB_1925525	Abcam
TLR4	sc-293072	AB_10611320	Santa Cruz Biotechnology
LAMP2 (GL2A7)	ab13524	AB_2134736	Abcam
LAMP1 (1D4B)	ab25245	AB_449893	Abcam
LC3A/B	12741	AB_2617131	Cell Signaling Technology Inc.
BACE-1 (D10E5)	5606	AB_1903900	Cell Signaling Technology Inc.
IBA-1	019–19741	AB_839504	Wako
HIF-1α	14179	AB_2622225	Cell Signaling Technology Inc.
PSD-95 (23H23L19)	700902	AB_2532348	Thermo Fisher Scientific
Synaptotagmin-1	14558	AB_2798510	Cell Signaling Technology Inc.
Homer 1	8231	AB_10858221	Cell Signaling Technology Inc.
Rim-1	140003	AB_887774	Synaptic Systems
CD68	76437	AB_2799882	Cell Signaling Technology Inc.
mTOR (7C10)	2983	AB_2105622	Cell Signaling Technology Inc.
p-mTOR (Ser ²⁴⁴⁸)	5536	AB_10691552	Cell Signaling Technology Inc.
p62/SQSTM1	ab155686	AB_2847961	Abcam

Scientific) with continuous perfusion of artificial cerebrospinal fluid and bubbling of 95% O₂/5% CO₂. The device has an array arranged in an 8 × 8 pattern of 64 planar microelectrodes across a hippocampal slice. Each electrode used for data acquisition and analysis was 20 μm × 20 μm with an interelectrode distance of 150 μm. Schaffer collateral-to-CA1 synapses were typically analyzed for LTP assays. Field excitatory postsynaptic potentials (fEPSPs) caused by stimulation were recorded at a 20-kHz sampling rate within the CA1 subregion of the hippocampus. Control fEPSPs were recorded for at least 10 min before the conditioning stimulation using a response ~50% of the maximum. After a stable baseline was established, LTP was induced with three trains of 100 Hz for 1 s with an intertrain interval of 20 s. Field potential amplitudes were then measured. Data are expressed as means ± SEM. Synaptic strength was evaluated by measuring changes in the fEPSP amplitude relative to baseline. Statistics were calculated by Student's *t* tests.

Generation of microglial *Bace-1* conditional knockout mice

Tamoxifen-inducible microglia-specific *Bace-1* deletion was achieved by breeding microglia-specific B6.129P2(26)Cx3cr1^{tm2.1(cre/ERT2)Litt}/WgnJ (JAX stock no. 020940, the Jackson Laboratory) with *Bace-1* conditional mice (*Bace-1*^{f/f}) carrying loxP-flanked genes as previously

described (8). The heterozygous mice were further bred to obtain a colony with the following genotype: Cx3cr1^{Cre/ERT2}; *Bace-1*^{f/f}. At 2 months, the *Bace-1* deletion in microglia was initiated by injecting tamoxifen intraperitoneally at 100 mg/kg for five consecutive days. The level of BACE-1 was examined by isolating microglia, and the extent of BACE-1 deletion was examined by immunoblotting. All animal studies were conducted according to the approved procedures by the Institutional Animal Care and Use Committee University of Connecticut Health.

Contextual fear conditioning test

The contextual fear conditioning test is conducted over a span of 3 days. On day one, which was also the conditioning period, the mouse was placed in the conditioning chamber (26 cm by 34 cm by 29 cm; Med Associates) for 3 min, before being exposed to conditional stimuli in the form of two sound exposures 1 min apart lasting for 30 s each (2800 Hz and 85 dB). During the last 2 s of the conditioning stimulus, the mice were given a 0.75-mA continuous foot shock (unconditioned stimulus). The mouse was removed from the chamber 30 s after the last foot shock and placed back in its original cage. On the second day, mice were tested for their contextual memory in the same chamber for 3 min without either sound or foot shock.

The freezing response was defined as the percentage of time a mouse remained motionless (intervals of 5 s with the exception of respiration-related movements). On the third day, mice were tested for cue-based memory for 5 min in a different chamber environment (different background) with the two 30-s sound stimuli 1 min apart without any foot shock. Fear-based memory was measured as the percentage of freezing, both pretone and posttone.

Y-maze test

Spatial working memory and reference memory were analyzed using the standard Y-maze test. The Y-maze consisted of three symmetrical arms separated by 120°. Mice were placed in the center of the Y-maze and were allowed to explore freely for 5 min while the activity was recorded and analyzed by a computer program (Viewer3, BIOSERVE, St. Augustin, Germany). Alternations were considered to be completed when a mouse performed successive entries into three different arms of the Y-maze (ABC, BCA, and so on). Percentage alternations was calculated as the ratio of actual alternations and maximum possible alternations (the total number of arm entries – 2) × 100, as follows

$$\% \text{ alternation} = [(\text{no. of alternations}) / (\text{total no. of arm entries} - 2)] \times 100$$

Open-field test

A square open-field apparatus with dimensions of 100-cm-diameter and 55-cm-high sidewalls was used to determine locomotor and anxiety-like behavior. Mice were released in the middle of the arena, and recording was started 1 min after release and continued for another 10 min. Mouse movement was traced in the open field by a computer-based video tracking system (ANY-maze software, San Diego Instruments, USA). Activity measured included total distance traveled, time spent in the center and corners, the total number of entries in the center, and the distance traveled in both the center and around the corners. Statistics were calculated with Student's *t* tests.

CRISPR null of BACE-1 in BV-2 cells

Guide RNAs (gRNAs) were designed to specifically cut in the second exon of the *Bace-1* gene in the mouse genome (Ensembl sequences ENSMUSG00000032086). gRNA was designed for high specificity and to guard against genome-wide off-target effects using <https://chopchop.cbu.uib.no/>. Oligos containing the gRNA sequence were cloned into lentiCRISPR v2 (Addgene plasmid) (38). Scramble gRNA was also designed to be used as a control in this study. gRNAs were designed to bind to the genome in a position flanked by an NGG at the 3' end. Oligos were ordered (26) and phosphorylated/annealed. The annealed gRNA oligos were cloned into the lentiCRISPR v2 plasmid digested with BsmB1 to create the appropriate overhangs. The following primers were used: gRNA for *Bace-1* (5'-TCCTGCATCGCTACTACCAG-3') and gRNA for scramble (5'CAGTCGGCGTCATCATGAT-3').

Plasmids were sequenced to verify correct insertion of gRNAs. Lentivirus was made using the packaging plasmids pspAX2 and pMD2.G (Addgene plasmid no. 12260 and Addgene plasmid no. 12259, gift of D. Trono) into human embryonic kidney 293FT cells using Lipofectamine 2000 (Thermo Fisher Scientific). Virus was harvested at 48 hours after transfection.

BV-2 cells were plated and transduced by the lentivirus. Forty-eight hours after transduction, puromycin was added to the culture at 4 ng/μl to select for lentiCRISPR integration. After selection, a group of bulk cells were tested using a T7E1 assay to verify the creation

of insertions or deletions (INDELs). Once INDELs were verified, cells were plated sparsely as single cells and allowed to create colonies. Colonies were isolated into 24-well plates and allowed to expand. The plate was duplicated, one set of wells were lysed, and genomic DNA was isolated. The region of CRISPR binding was amplified by polymerase chain reaction (PCR) and sequenced by Sanger sequencing. Sequences were analyzed to identify frameshifts in exon 2. Cells with different INDELs on each allele were analyzed using TIDE analysis 2 using chromatograms of the edited samples comparing to the WT cells.

Clones that showed frameshift INDELs on both alleles leading to nonsense and early termination were expanded for use in this study.

Primers used for analysis are as follows: *Bace-1* mouse exon 2 PCR [GACGATCAGGTGACAGGAAA (forward)], BACE mouse ex2 pcr (reverse), BACE1 mouse exon 2 PCR [5'-GACGATCAGGTGACAGGAAA-3' (forward)], BACE mouse exon 2 PCR [5'-TGGTTCAT-GTTCTGCTCTGG-3' (reverse)], and BACE mouse exon2 seq [5'-ACAGACAGACGCAAGTGCAG-3' (forward)].

Statistical analysis

Results are expressed as means ± SEM. The statistical analyses were performed using GraphPad Prism 6.0 software (GraphPad Software, San Diego). Student's *t* tests were used to compare between two groups. Multiple group analyses were performed by one-way analysis of variance (ANOVA), followed by Tukey's post hoc test. Differences with **P* < 0.05, ***P* < 0.01, and ****P* < 0.001 were considered significant.

SUPPLEMENTARY MATERIALS

Supplementary material for this article is available at <https://science.org/doi/10.1126/sciadv.abo3610>

[View/request a protocol for this paper from Bio-protocol.](#)

REFERENCES AND NOTES

- C. R. Jack Jr., D. A. Bennett, K. Blennow, M. C. Carrillo, B. Dunn, S. B. Haeberlein, D. M. Holtzman, W. Jagust, F. Jessen, J. Karlawish, E. Liu, J. L. Molinuevo, T. Montine, C. Phelps, K. P. Rankin, C. C. Rowe, P. Scheltens, E. Siemers, H. M. Snyder, R. Sperling; Contributors, NIA-AA Research Framework: Toward a biological definition of Alzheimer's disease. *Alzheimers Dement.* **14**, 535–562 (2018).
- M. F. Egan, J. Kost, T. Voss, Y. Mukai, P. S. Aisen, J. L. Cummings, P. N. Tariot, B. Vellas, C. H. van Dyck, M. Boada, Y. Zhang, W. Li, C. Furtek, E. Mahoney, L. Harper Mozley, Y. Mo, C. Sur, D. Michelson, Randomized trial of verubecestat for prodromal Alzheimer's disease. *N. Engl. J. Med.* **380**, 1408–1420 (2019).
- A. M. Wessels, P. N. Tariot, J. A. Zimmer, K. J. Selzler, S. M. Bragg, S. W. Andersen, J. Landry, J. H. Krull, A. M. Downing, B. A. Willis, S. Shcherbinin, J. Mullen, P. Barker, J. Schumi, C. Shering, B. R. Matthews, R. A. Stern, B. Vellas, S. Cohen, E. MacSweeney, M. Boada, J. R. Sims, Efficacy and safety of lanabecestat for treatment of early and mild Alzheimer disease: The AMARANTH and DAYBREAK-ALZ randomized clinical trials. *JAMA Neurol.* **77**, 199–209 (2020).
- B. Das, R. Yan, A close look at BACE1 inhibitors for Alzheimer's disease treatment. *CNS Drugs* **33**, 251–263 (2019).
- B. P. Imbimbo, M. Watling, Investigational BACE inhibitors for the treatment of Alzheimer's disease. *Expert Opin. Investig. Drugs* **28**, 967–975 (2019).
- C. Sur, J. Kost, D. Scott, K. Adamczuk, N. C. Fox, J. L. Cummings, P. N. Tariot, P. S. Aisen, B. Vellas, T. Voss, E. Mahoney, Y. Mukai, M. E. Kennedy, C. Lines, D. Michelson, M. F. Egan, BACE inhibition causes rapid, regional, and non-progressive volume reduction in Alzheimer's disease brain. *Brain* **143**, 3816–3826 (2020).
- M. H. Ou-Yang, J. E. Kurz, T. Nomura, J. Popovic, T. W. Rajapaksha, H. Dong, A. Contractor, D. M. Chetkovich, W. G. Tourtellotte, R. Vassar, Axonal organization defects in the hippocampus of adult conditional BACE1 knockout mice. *Sci. Transl. Med.* **10**, eaao5620 (2018).
- X. Hu, B. Das, H. Hou, W. He, R. Yan, BACE1 deletion in the adult mouse reverses preformed amyloid deposition and improves cognitive functions. *J. Exp. Med.* **215**, 927–940 (2018).
- H. Wang, L. Song, F. Laird, P. C. Wong, H. K. Lee, BACE1 knock-outs display deficits in activity-dependent potentiation of synaptic transmission at mossy fiber to CA3 synapses in the hippocampus. *J. Neurosci.* **28**, 8677–8681 (2008).

10. S. Lombardo, M. Chiacchiaretta, A. Tarr, W. Kim, T. Cao, G. Sigal, T. W. Rosahl, W. Xia, P. G. Haydon, M. E. Kennedy, G. Tesco, BACE1 partial deletion induces synaptic plasticity deficit in adult mice. *Sci. Rep.* **9**, 19877 (2019).
11. M. Vnencak, M. L. Scholvinck, S. W. Schwarzscher, T. Deller, M. Willem, P. Jedlicka, Lack of β -amyloid cleaving enzyme-1 (BACE1) impairs long-term synaptic plasticity but enhances granule cell excitability and oscillatory activity in the dentate gyrus *in vivo*. *Brain Struct. Funct.* **224**, 1279–1290 (2019).
12. K. Zhu, F. Peters, S. Filser, J. Herms, Consequences of pharmacological BACE inhibition on synaptic structure and function. *Biol. Psychiatry* **84**, 478–487 (2018).
13. M. E. Kennedy, A. W. Stamford, X. Chen, K. Cox, J. N. Cumming, M. F. Dockendorf, M. Egan, L. Ereshesky, R. A. Hodgson, L. A. Hyde, S. Jhee, H. J. Kleijn, R. Kavelkar, W. Li, B. A. Mattson, H. Mei, J. Palusz, J. D. Scott, M. Tanen, M. D. Troyer, J. L. Tseng, J. A. Stone, E. M. Parker, M. S. Forman, The BACE1 inhibitor verubecestat (MK-8931) reduces CNS β -amyloid in animal models and in Alzheimer's disease patients. *Sci. Transl. Med.* **8**, 363ra150 (2016).
14. R. Li, K. Lindholm, L. B. Yang, X. Yue, M. Citron, R. Yan, T. Beach, L. Sue, M. Sabbagh, H. Cai, P. Wong, D. Price, Y. Shen, Amyloid beta peptide load is correlated with increased beta-secretase activity in sporadic Alzheimer's disease patients. *Proc. Natl. Acad. Sci. U.S.A.* **101**, 3632–3637 (2004).
15. P. C. Kandalepas, K. R. Sadleir, W. A. Eimer, J. Zhao, D. A. Nicholson, R. Vassar, The Alzheimer's β -secretase BACE1 localizes to normal presynaptic terminals and to dystrophic presynaptic terminals surrounding amyloid plaques. *Acta Neuropathol.* **126**, 329–352 (2013).
16. N. Singh, M. R. Benoit, J. Zhou, B. Das, J. Davila-Velderrain, M. Kellis, L.-H. Tsai, X. Hu, R. Yan, BACE-1 inhibition facilitates the transition from homeostatic microglia to DAM-1. *Sci. Adv.* **8**, eab01286 (2022).
17. H. Oakley, S. L. Cole, S. Logan, E. Maus, P. Shao, J. Craft, A. Guillozet-Bongaarts, M. Ohno, J. Disterhoft, E. L. Van, R. Berry, R. Vassar, Intraneuronal β -amyloid aggregates, neurodegeneration, and neuron loss in transgenic mice with five familial Alzheimer's disease mutations: Potential factors in amyloid plaque formation. *J. Neurosci.* **26**, 10129–10140 (2006).
18. S. H. Baik, S. Kang, W. Lee, H. Choi, S. Chung, J. I. Kim, I. Mook-Jung, A breakdown in metabolic reprogramming causes microglia dysfunction in Alzheimer's disease. *Cell Metab.* **30**, 493–507.e6 (2019).
19. D. DeWaal, V. Nogueira, A. R. Terry, K. C. Patra, S. M. Jeon, G. Guzman, J. Au, C. P. Long, M. R. Antoniewicz, N. Hay, Hexokinase-2 depletion inhibits glycolysis and induces oxidative phosphorylation in hepatocellular carcinoma and sensitizes to metformin. *Nat. Commun.* **9**, 446 (2018).
20. A. Latif-Hernandez, V. Sabanov, T. Ahmed, K. Craessaerts, T. Saito, T. Saido, D. Balschun, The two faces of synaptic failure in App^{NL-GF} knock-in mice. *Alzheimers Res. Ther.* **12**, 100 (2020).
21. J. M. Long, D. M. Holtzman, Alzheimer disease: An update on pathobiology and treatment strategies. *Cell* **179**, 312–339 (2019).
22. L. Bertram, R. E. Tanzi, Alzheimer disease risk genes: 29 and counting. *Nat. Rev. Neurol.* **15**, 191–192 (2019).
23. D. M. Walsh, D. J. Selkoe, Amyloid β -protein and beyond: The path forward in Alzheimer's disease. *Curr. Opin. Neurobiol.* **61**, 116–124 (2020).
24. R. Vassar, Editorial: Implications for BACE1 inhibitor clinical trials: Adult conditional BACE1 knockout mice exhibit axonal organization defects in the hippocampus. *J. Prev. Alzheimers Dis.* **6**, 78–84 (2019).
25. C. Villegas-Llerena, A. Phillips, P. Garcia-Reitboeck, J. Hardy, J. M. Pocock, Microglial genes regulating neuroinflammation in the progression of Alzheimer's disease. *Curr. Opin. Neurobiol.* **36**, 74–81 (2016).
26. R. Sims, S. J. van der Lee, A. C. Naj, C. Bellenguez, N. Badarinayaran, J. Jakobsson, B. W. Kunkle, A. Boland, R. Raybould, J. C. Bis, E. R. Martin, B. Grenier-Boley, S. Heilmann-Heimbach, V. Chouraki, A. B. Kuzma, K. Sleegers, M. Vronskaya, A. Ruiz, R. R. Graham, R. Olaso, P. Hoffmann, M. L. Grove, B. N. Vardarajan, M. Hiltunen, M. M. Nothen, C. C. White, K. L. Hamilton-Nelson, J. Epelbaum, W. Maier, S. H. Choi, G. W. Beecham, C. Dulary, S. Herms, A. V. Smith, C. F. Funk, C. Derbois, A. J. Forstner, S. Ahmad, H. Li, D. Bacq, D. Harold, C. L. Satizabal, O. Valladares, A. Squassina, R. Thomas, J. A. Brody, L. Qu, P. Sanchez-Juan, T. Morgan, F. J. Wolters, Y. Zhao, F. S. Garcia, N. Denning, M. Fornage, J. Malamon, M. C. D. Naranjo, E. Majounie, T. H. Mosley, B. Dombroski, D. Wallon, M. K. Lupton, J. Dupuis, P. Whitehead, L. Fratiglioni, C. Medway, X. Jian, S. Mukherjee, L. Keller, K. Brown, H. Lin, L. B. Cantwell, F. Panza, B. McGuinness, S. Moreno-Grau, J. D. Burgess, V. Solfrizzi, P. Proitsi, H. H. Adams, M. Allen, D. Seripa, P. Pastor, L. A. Cupples, N. D. Price, D. Hannequin, A. Frank-Garcia, D. Levy, P. Chakrabarty, P. Caffarra, I. Giegling, A. S. Beiser, V. Giedraitis, H. Hampel, M. E. Garcia, X. Wang, L. Lannfelt, P. Mecocci, G. Eiriksdottir, P. K. Crane, F. Pasquier, V. Boccardi, I. Henandez, R. C. Barber, M. Scherer, L. Tarraga, P. M. Adams, M. Leber, Y. Chen, M. S. Albert, S. Riedel-Heller, V. Emilson, D. Beekly, A. Braae, R. Schmidt, D. Blacker, C. Masullo, H. Schmidt, R. S. Doody, G. Spalletta, W. T. Longstreth Jr., T. J. Fairchild, P. Bossu, O. L. Lopez, M. P. Frosch, E. Sacchinielli, B. Ghetti, Q. Yang, R. M. Huebinger, F. Jessen, S. Li, M. I. Kamboh, J. Morris, O. Sotolongo-Grau, M. J. Katz, C. Corcoran, M. Dunstan, A. Braddell, C. Thomas, A. Meggy, R. Marshall, A. Gerrish, J. Chapman, M. Aguilar, S. Taylor, M. Hill, M. D. Fairten, A. Hodges, B. Vellas, H. Soininen, I. Kloszewska, M. Daniellidou, J. Uphill, Y. Patel, J. T. Hughes, J. Lord, J. Turton, A. M. Hartmann, R. Cecchetti, C. Fenoglio, M. Serpente, M. Arcaro, C. Caltagirone, M. D. Orfei, A. Ciaramella, S. Pichler, M. Mayhaus, W. Gu, A. Lleo, J. Fortea, R. Blesa, I. S. Barber, K. Brookes, C. Cupidi, R. G. Maletta, D. Carroll, S. Sorbi, S. Moebus, M. Urbano, A. Pilotto, J. Kornhuber, P. Bosco, S. Todd, D. Craig, J. Johnston, M. Gill, B. Lawlor, A. Lynch, N. C. Fox, J. Hardy, R. L. Albin, L. G. Apostolova, S. E. Arnold, S. Asthana, C. S. Atwood, C. T. Baldwin, L. L. Barnes, S. Barral, T. G. Beach, J. T. Becker, E. H. Bigio, T. D. Bird, B. F. Boeve, J. D. Bowen, A. Boxer, J. R. Burke, J. M. Burns, J. D. Buxbaum, N. J. Cairns, C. Cao, C. S. Carlson, C. M. Carlsson, R. M. Carney, M. M. Carrasquillo, S. L. Carroll, C. C. Diaz, H. C. Chui, D. G. Clark, D. H. Cribbs, E. A. Crocco, C. DeCarli, M. Dick, R. Duara, D. Evans, K. M. Faber, K. B. Fallon, D. W. Fardo, M. R. Farlow, S. Ferris, T. M. Foroud, D. R. Galasko, M. Gearing, D. H. Geschwind, J. R. Gilbert, N. R. Graff-Radford, R. C. Green, J. H. Growdon, R. L. Hamilton, L. E. Harrell, L. S. Honig, M. J. Huentelman, C. M. Hulette, B. T. Hyman, G. P. Jarvik, E. Abner, L. W. Jin, G. Jun, A. Karydas, J. A. Kaye, R. Kim, N. W. Kowall, J. H. Kramer, F. M. LaFerla, J. J. Lah, J. B. Leverenz, A. I. Levey, G. Li, A. P. Lieberman, K. L. Lunetta, C. G. Lyketsos, D. C. Marson, F. Martiniuk, D. C. Mash, E. Masliah, W. C. McCormick, S. M. McCurry, A. N. McDavid, A. C. McKee, M. Mesulam, B. L. Miller, C. A. Miller, J. W. Miller, J. C. Morris, J. R. Murrell, A. J. Myers, S. O'Bryant, J. M. Olichney, V. S. Pankratz, J. E. Parisi, H. L. Paulson, W. Perry, E. Peskind, A. Pierce, W. W. Poon, H. Potter, J. F. Quinn, A. Raj, M. Raskind, B. Reisberg, C. Reitz, J. M. Ringman, E. D. Roberson, E. Rogaeva, H. J. Rosen, R. N. Rosenberg, M. A. Sager, A. J. Saykin, J. A. Schneider, L. S. Schneider, W. W. Seeley, A. G. Smith, J. A. Sonnen, S. Spina, R. A. Stern, R. H. Swerdlow, R. E. Tanzi, T. A. Thornton-Wells, J. Q. Trojanowski, J. C. Troncoso, V. M. Van Deerlin, L. J. Van Eldik, H. V. Vinters, J. P. Vonsattel, S. Weintraub, K. A. Welsh-Bohmer, K. C. Wilhelmsen, J. Williamson, T. S. Wingo, R. L. Woltjer, C. B. Wright, C. E. Yu, L. Yu, F. Garzia, F. Golamau, G. Septier, S. Engelborghs, R. Vandenberghe, P. P. De Deyn, C. M. Fernandes, Y. A. Benito, H. Thonberg, C. Forsell, L. Lilius, A. Kinjhult-Stahlbom, L. Kilander, R. Brundin, L. Concari, S. Helisalmi, A. M. Koivisto, A. Haapasalo, V. Dermecourt, N. Fievet, O. Hanon, C. Dufouil, A. Brice, K. Ritchie, B. Dubois, J. J. Himali, C. D. Keene, J. Tschanz, A. L. Fitzpatrick, W. A. Kukull, M. Norton, T. Aspelund, E. B. Larson, R. Munger, J. I. Rotter, R. B. Lipton, M. J. Bullido, A. Hofman, T. J. Montine, E. Coto, E. Boerwinkle, R. C. Petersen, V. Alvarez, F. Rivadeneira, E. M. Reiman, M. Gallo, C. J. O'Donnell, J. S. Reisch, A. C. Brunni, D. R. Royall, M. Dichgans, M. Sano, D. Galimberti, P. S. George-Hyslop, E. Scarpini, D. W. Tsuang, M. Mancuso, U. Bonuccelli, A. R. Winslow, A. Daniele, C. K. Wu; GERAD/PERADES, CHARGE, ADGC, EADI, O. Peters, B. Nacmias, M. Riemenschneider, R. Heun, C. Brayne, D. C. Rubinsztein, J. Bras, R. Guerreiro, A. Al-Chalabi, C. E. Shaw, J. Collinge, D. Mann, M. Tsolaki, J. Clarimon, R. Sussams, S. Lovestone, M. C. O'Donovan, M. J. Owen, T. W. Behrens, S. Mead, A. M. Goate, A. G. Uitterlinden, C. Holmes, C. Cruchaga, M. Ingelsson, D. A. Bennett, J. Powell, T. E. Golde, C. Graff, P. L. De Jager, K. Morgan, N. Ertekin-Taner, O. Combarros, B. M. Psaty, P. Passmore, S. G. Younkin, C. Berr, V. Gudnason, D. Rujescu, D. W. Dickson, J. F. Dartigues, A. L. De Stefano, S. Ortega-Cubero, H. Hakonarson, D. Campion, M. Boada, J. K. Kauwe, L. A. Farrer, C. Van Broeckhoven, M. A. Ikram, L. Jones, J. L. Haines, C. Tzourio, L. J. Launer, V. Escott-Price, R. Mayeux, J. F. Deleuze, N. Amin, P. A. Holmans, M. A. Pericak-Vance, P. Amouyel, C. M. van Duijn, A. Ramirez, L. S. Wang, J. C. Lambert, S. Seshadri, J. Williams, G. D. Schellenberg, Rare coding variants in PLCG2, ABI3, and TREM2 implicate microglial-mediated innate immunity in Alzheimer's disease. *Nat. Genet.* **49**, 1373–1384 (2017).
27. R. Guerreiro, A. Wojtas, J. Bras, M. Carrasquillo, E. Rogaeva, E. Majounie, C. Cruchaga, C. Sassi, J. S. Kauwe, S. Younkin, L. Hazrati, J. Collinge, J. Pocock, T. Lashley, J. Williams, J. C. Lambert, P. Amouyel, A. Goate, R. Rademakers, K. Morgan, J. Powell, P. St George-Hyslop, A. Singleton, J. Hardy; Alzheimer Genetic Analysis Group, *TREM2* Variants in Alzheimer's disease. *N. Engl. J. Med.* **368**, 117–127, (2013).
28. T. Jonsson, H. Stefansson, D. S. Ph, I. Jonsdottir, P. V. Jonsson, J. Snaedal, S. Bjornsson, J. Huttonlocher, A. I. Levey, J. J. Lah, D. Rujescu, H. Hampel, I. Giegling, O. A. Andreassen, K. Engedal, I. Ulstein, S. Djurovic, C. Ibrahim-Vervaas, A. Hofman, M. A. Ikram, C. M. van Duijn, U. Thorsteinsdottir, A. Kong, K. Stefansson, Variant of *TREM2* associated with the risk of Alzheimer's disease. *N. Engl. J. Med.* **368**, 107–116 (2013).
29. G. Novak, J. R. Stretter, M. Timmers, D. Henley, H. R. Brashear, J. Bogert, A. Russu, L. Janssens, I. Tesseur, L. Tritsman, L. Van Nueten, S. Engelborghs, Long-term safety and tolerability of atabecestat (JNJ-54861911), an oral BACE1 inhibitor, in early Alzheimer's disease spectrum patients: A randomized, double-blind, placebo-controlled study and a two-period extension study. *Alzheimers Res. Ther.* **12**, 58 (2020).
30. B. Das, N. Singh, A. Y. Yao, J. Zhou, W. He, X. Hu, R. Yan, BACE1 controls synaptic function through modulating release of synaptic vesicles. *Mol. Psychiatry* **26**, 6394–6410 (2021).
31. B. Dislich, F. Wohlrab, T. Bachhuber, S. Mueller, P. H. Kuhn, S. Hogl, M. Meyer-Luehmann, S. F. Lichtenhaller, Label-free quantitative proteomics of mouse cerebrospinal fluid detects β -site APP cleaving enzyme (BACE1) protease substrates *in vivo*. *Mol. Cell. Proteomics* **14**, 2550–2563 (2015).
32. H. Keren-Shaul, A. Spinrad, A. Weiner, O. Matcovitch-Natan, R. Dvir-Szternfeld, T. K. Ulland, E. David, K. Baruch, D. Lara-Astasio, B. Toth, S. Itzkovitz, M. Colonna, M. Schwartz, I. Amit, A unique microglia type associated with restricting development of Alzheimer's disease. *Cell* **169**, 1276–1290.e17 (2017).

33. H. Mathys, C. Adaikkan, F. Gao, J. Z. Young, E. Manet, M. Hemberg, P. L. De Jager, R. M. Ransohoff, A. Regev, L. H. Tsai, Temporal tracking of microglia activation in neurodegeneration at single-cell resolution. *Cell Rep.* **21**, 366–380 (2017).
34. D. Mrdjen, A. Pavlovic, F. J. Hartmann, B. Schreiner, S. G. Utz, B. P. Leung, I. Lelios, F. L. Heppner, J. Kipnis, D. Merkler, M. Greter, B. Becher, High-dimensional single-cell mapping of central nervous system immune cells reveals distinct myeloid subsets in health, aging, and disease. *Immunity* **48**, 599 (2018).
35. H. Hampel, S. Lista, E. Vanmechelen, H. Zetterberg, F. S. Giorgi, A. Galgani, K. Blennow, F. Caraci, B. Das, R. Yan, A. Vergallo, β -Secretase1 biological markers for Alzheimer's disease: State-of-art of validation and qualification. *Alzheimers Res. Ther.* **12**, 130 (2020).
36. L. Rajendran, R. C. Paolicelli, Microglia-mediated synapse loss in Alzheimer's disease. *J. Neurosci.* **38**, 2911–2919 (2018).
37. X. Chen, A. Stoeck, S. J. Lee, I. Shih, M. M. Wang, T. L. Wang, Jagged1 expression regulated by Notch3 and Wnt/ β -catenin signaling pathways in ovarian cancer. *Oncotarget* **1**, 210–218 (2010).
38. O. Shalem, N. E. Sanjana, F. Zhang, High-throughput functional genomics using CRISPR-Cas9. *Nat. Rev. Genet.* **16**, 299–311 (2015).

Acknowledgments

Funding: R.Y. was supported by grants RF1AG058261, AG025493, NS074256, and AG046929 from the NIH. R.Y.'s laboratory was also supported by the Cure Alzheimer's Fund. B.D. was supported by a postdoctoral fellowship from the BrightFocus Foundation (A20201729F). We also thank the Bioinformatics Core at UConn Health for support. **Author contributions:** N.S. and R.Y. designed and initiated this study. N.S. conducted most of experiments and wrote the draft. N.S. and B.D. conducted behavioral experiments and B.D. for LTP experiments. J.Z. and X.H. helped some data analysis. R.Y. supervised the project and wrote the manuscript.

Competing interests: The authors declare that they have no competing interests. **Data and materials availability:** All data needed to evaluate the conclusions in the paper are present in the paper and/or the Supplementary Materials.

Submitted 28 January 2022

Accepted 7 June 2022

Published 20 July 2022

10.1126/sciadv.abo3610